Journal of Mathematical Biology (2026) 93:20
https://doi.org/10.1007/s00285-026-02432-z

Mathematical Biology

Global stability of an SIQR switched model with multiple two-threshold structures

Haifeng Wang[1] · **Yanni Xiao**[1] · **Xingfu Zou**[2]

Received: 7 October 2025 / Revised: 22 April 2026 / Accepted: 14 June 2026
© The Author(s), under exclusive licence to Springer-Verlag GmbH Germany, part of Springer Nature 2026

Abstract

Prevention and control strategies play an essential role in reducing new infections of infectious diseases, while uniform and instantaneous responses to disease outbreaks are assumed in traditional epidemic models. To model the adaptive public health policies that account for hysteresis effects and heterogeneous control measures, we proposed an SIQR epidemic model with multiple two-threshold structures to describe the prevalence-dependent real-time control strategies. The formulated model incorporated the Preisach operator which effectively characterizes time-varying control strategies that depend on the historical evolution of a disease. We established the global stability of this steady-state set through an innovative analytical approach by constructing a series of Lyapunov functions corresponding to different branches of the hysteresis operator. Specifically, our results indicate that: (i) heterogeneity facilitates the convergence of system trajectories to a point within the continuum of steady-state, and (ii) greater heterogeneity leads to higher peaks of infected individuals during the evolution of an epidemic and more severe disease prevalence in the long term. Our findings reveal that the hysteresis phenomenon in control events may lead to existence of a continuum of endemic equilibria, significantly altering the effectiveness of disease suppression strategies. These results provide a theoretical foundation for designing adaptive control policies, emphasizing the importance of incorporating past intervention effects in epidemic modeling.

Keywords Switched model · Multiple two-threshold · Heterogeneous control strategy · Continuum set of equilibria · Hysteresis operator · Global stability

Mathematics Subject Classification 34D23 · 92D30 · 92D25

✉ Yanni Xiao
yxiao@mail.xjtu.edu.cn

[1] School of Mathematics and Statistics, Xi'an Jiaotong University, Xi'an 710049, China

[2] Department of Mathematics, University of Western Ontario, London N6A 5B7, Canada

Published online: 18 July 2026

1 Introduction

The development and implementation of effective disease prevention and control strategies constitute a cornerstone of modern public health. Such strategies not only mitigate morbidity and mortality associated with infectious diseases but also play a decisive role in reducing the long-term societal and economic consequences of epidemics. Interventions including vaccination programs, early diagnostic screening, contact tracing, quarantine measures, and health communication campaigns are critical for interrupting transmission chains and protecting high-risk populations, such as influenza, Ebola, childhood disease and COVID-19 (Feng and Thieme 1995; Ll and Feng 2000; Herbert et al. 2002; Erdem et al. 2017; Mondaini 2018; Odagaki 2020; Wang et al. 2023; Pinto et al. 2024; Wang et al. 2026).

The epidemiological models is essential for understanding the dynamics of infectious diseases, especially in the context of public health management and intervention strategies. Traditional infectious disease models generally assume that control measures are applied continuously throughout the transmission process and remain of constant intensity. In practice, however, most interventions can only be implemented for a limited period, such as community isolation and business restriction, due to non-pharmaceutical interventions have a significant impact on economic and social aspects (Fairlie 2020; Wang et al. 2022). Given these constraints, many intervention programs implemented by health authorities to mitigate disease transmission (Wilder-Smith et al. 2020) can, at least temporarily, be modelled as threshold-based or event-triggered control strategies (Rachinskii and Rouf 2022; Huang and Wang 2024). In such frameworks, the timing of both activation and suspension of control measures becomes critical. For instance, Wang and Xiao (2025) analyzed an SIQR model incorporating a single two-threshold structure, in which interventions are initiated once a key variable (such as the number of infectious individuals) exceeds a specified upper threshold and are lifted when it falls below a lower, safer level. Their research has demonstrated that two-threshold strategies can effectively suppress infection prevalence during the course of an epidemic. Nonetheless, modeling scenarios involving the combined application of multiple interventions, as well as dynamically adjusting the intensity of individual measures in response to epidemic progression, poses significant analytical challenges. In particular, the comprehensive dynamics of the epidemic models subject to heterogeneous control strategies remains unclear and falls within the scope of this study.

We note that when the thresholds for triggering/suspending the control strategies differ, hysteresis effects naturally emerge, thereby shaping the qualitative features of epidemic dynamics (Krasnosel'skii and Pokrovskii 1989; d'Onofrio and Piero 2009). These modes, which may include varying levels of quarantine enforcement, testing rates, and social distancing measures, create a complex dynamical system where different regions or populations may experience different rates of intervention. In such models, the effectiveness of control strategies often depends on the thresholds of intervention and feedback loops within the system. Hysteresis, a term commonly used in physics and engineering (Meza and Bhaya 2010), refers to systems where the current state depends not only on the present conditions but also on the past history of the system (Visintin 1994). This concept can be applied to control strategies in epidemic

models, where the effectiveness of control measures (such as quarantine and isolation) may depend on the history of disease spread and previous interventions (Schelling 1971). The incorporation of hysteresis allows us for a more realistic representation of control strategies, where interventions are delayed or their effects are less immediate due to social, economic, or logistical factors. Indeed, the concept of hysteresis operator has been used to study the dynamics of some epidemiological models (Pimenov et al. 2012; Kopfová et al. 2021; Rachinskii and Rouf 2022; Guan et al. 2024) and predator-prey models (Krejči et al. 2012; Pimenov and Rachinskii 2014; Pimenov et al. 2015; Gurevich and Rachinskii 2015; Pimenov et al. 2017).

In this study we extend the SIQR model with a single two-threshold structure (Wang and Xiao 2025), by incorporating multiple two-threshold structures, including finite and infinite cases, to describe the impacts of heterogeneous control strategies. These can be naturally represented using discrete and continuous Preisach operators that induces hysteresis effects due to heterogeneous control strategies. In the context of epidemic models, this could represent situations where the effectiveness of quarantine measures or vaccination campaigns depends on the past levels of disease spread, the history of intervention, and social response to past outbreaks. We aim to understand the influence of past disease dynamics and control actions on the long-term dynamics. The global dynamics of such a model is crucial for understanding whether interventions can successfully eliminate or control the epidemic, and how the system responds to varying intensities of control over time.

This paper is organized as follows. Section 2 formulates an SIQR model with multiple two-threshold structures for finite and infinite cases. In Sect. 3, we present some preliminaries: the properties of continuous Preisach operator, the extended phase space and transform the SIQR model into an autonomous switched system. Global stability results are given in Sect. 4 and a detailed proof procedure is provided in Appendices, by constructing a series of Lyapunov functions with respect to different branches of the hysteresis operator. Some discussions in Sect. 5.

2 Modeling

To examine the influence of memory-dependent hysteresis control strategies on epidemic dynamics, we begin with the SIQR model incorporating a single two-threshold structure (Wang and Xiao 2025). This framework is then extended to SIQR models with finite and infinite two-threshold structures, enabling the characterization of real-time variations in isolation intensity throughout the course of disease evolution.

We consider a population that is divided into four different compartments of individuals: susceptible (S), infected (I), quarantined/isolated (Q) and recovered (R). Assuming that all offspring are born as susceptible and the birth/death rate in each group is the same. This assumption together with the assumption that the disease is not fatal (i.e., it does not cause death), the total population $N = S + I + Q + R$ remains a constant. Without loss of generality, we have chosen the scaling so that $N = 1$, and consequently S, I, Q and R denote the fractions of the corresponding subpopulations. We consider the following epidemiological model

$$\begin{cases} \dfrac{dS}{dt} = \mu - \dfrac{\beta SI}{1+\sigma S} - \mu S, \\ \dfrac{dI}{dt} = \dfrac{\beta SI}{1+\sigma S} - (\gamma_1 + \mu)I - v(t)I, \\ \dfrac{dQ}{dt} = v(t)I - (\gamma_2 + \mu)Q, \\ \dfrac{dR}{dt} = \gamma_1 I + \gamma_2 Q - \mu R, \end{cases} \tag{1}$$

with simple demographical factors and a feedback loop, which characterizes the dependence of the isolation intensity $v(t)$ on the current and past values of the proportion of infected individuals $I(t)$ (or prevalence of infection). Here $\mu > 0$ and $\beta > 0$ indicate the birth/death rate and transmission rate, respectively. And $\gamma_i > 0 (i = 1, 2)$ represents the recovery rate of infected and quarantined compartments, respectively. In large susceptible populations, a substantial fraction of individuals may adopt self-protective measures (e.g., avoiding crowded environments, mask usage, or vaccination), thereby reducing their likelihood of effective contact with infectious individuals. As a result, the effective incidence does not scale linearly with the total susceptible population. This saturation effect is represented in the incidence function $\beta SI/(1+\sigma S)$ with saturation rate σ induced by susceptible individuals taking protective measures against infection. Regardless of the specific dependence of v on I, we observe that the Q and R compartments do not influence the first two equations of model (1). Therefore, our analysis can be restricted to the following reduced model

$$\begin{cases} \dfrac{dS}{dt} = \mu - \dfrac{\beta SI}{1+\sigma S} - \mu S, \\ \dfrac{dI}{dt} = \dfrac{\beta SI}{1+\sigma S} - \delta I - v(t)I, \end{cases} \tag{2}$$

where $\delta = \gamma_1 + \mu$. Note that the region

$$\Omega = \{(S, I) \in \mathbb{R}^2_+ \mid S \geq 0, I \geq 0, S + I \leq 1\} \tag{3}$$

is a positive invariant set. Therefore, we will restrict our analysis to solutions within Ω. Specifically, within this region, we have $S' = \mu > 0$ for $S = 0$, $I' \leq (\beta - \delta)I$ and $I' = 0$ for $I = 0$, as well as

$$S' + I' \leq \mu - \mu S - \delta I < 0 \quad \text{for} \quad S + I = 1,$$

which implies that trajectories initiating from the region Ω remain within Ω. Moreover, when a constant isolation rate is implemented (i.e., $v(t) \equiv v > 0$), the basic reproduction number is given by

$$\mathcal{R}_0 = \frac{\beta}{(1+\sigma)(\delta + v)}.$$

The global dynamics of this basic system can then be determined accordingly. More precisely, if $\mathcal{R}_0 \leq 1$, the disease-free equilibrium $E_0 = (1, 0)$ is globally asymptotically stable in Ω; if $\mathcal{R}_0 > 1$, E_0 is a saddle point and an endemic equilibrium $E^* = (S^*, I^*)$ exists and is globally asymptotically stable in $\Omega_0 := \{(S, I) \in \mathbb{R}^2_+ \mid S > 0, I > 0, S + I \leq 1\}$, where

$$S^* = \frac{\delta + v}{\beta - \sigma(\delta + v)}, \quad I^* = \frac{\mu(1 - S^*)(1 + \sigma S^*)}{\beta S^*}. \tag{4}$$

Furthermore, the endemic equilibrium is of focus type if

$$\mu[(\beta - \sigma(\delta + v))^2 + \sigma(\delta + v)^2]^2 < 4(\delta + v)^2\beta(\beta - \sigma(\delta + v))(\beta - (1 + \sigma)(\delta + v)).$$

In this case, the disease dynamics approach the equilibrium through damped oscillations, indicating that the spread of the disease stabilizes in a fluctuating manner.

2.1 The switched system with single two-threshold

A switched system consists of two modes governed by (2), each characterized by a distinct isolation intensity, v_1 and v_2, with $0 \leq v_1 < v_2$. Here, v_1 is used when the disease is mild, while v_2 is applied when it is severe. Specifically, the evolution of infectious diseases is constrained by a two-threshold structure, k_* and k_{**}, satisfying $0 \leq k_* < k_{**} \leq 1$. Under this framework, the switched system consists of two different subsystems

$$\begin{cases} \dfrac{dS}{dt} = \mu - \dfrac{\beta SI}{1 + \sigma S} - \mu S, \\ \dfrac{dI}{dt} = \dfrac{\beta SI}{1 + \sigma S} - \delta I - v_1 I, \end{cases} \quad \text{if } I(t) < k_{**}, \tag{5}$$

with the switching manifold $I = k_{**}$ and

$$\begin{cases} \dfrac{dS}{dt} = \mu - \dfrac{\beta SI}{1 + \sigma S} - \mu S, \\ \dfrac{dI}{dt} = \dfrac{\beta SI}{1 + \sigma S} - \delta I - v_2 I, \end{cases} \quad \text{if } I(t) > k_*, \tag{6}$$

with the switching manifold $I = k_*$. In other words, suppose that the isolation rate $v(t)$ instantaneously switches from a lower value v_1 to a higher value v_2 when the proportion of infected individuals is up to the value $I = k_{**}$. And the isolation rate switches from v_2 to v_1 when the prevalence decreases down to the value $I = k_*$ (shown in Fig. 1). The biological significance of this switching mechanism lies in the fact that both the strengthening and weakening of isolation are triggered relatively late (Wang and Xiao 2025). Two subsystems (5) and (6) have the same disease-free equilibrium

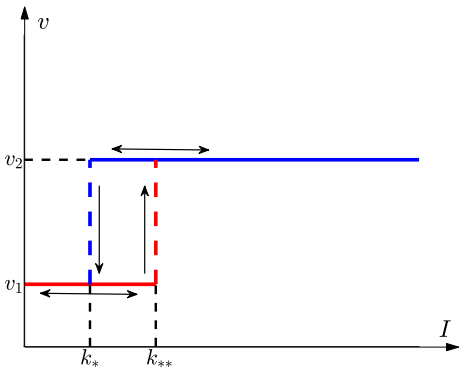


Fig. 1 Switching rule: the non-ideal relay operator. The input-output pair (I, v) always lies on one of two horizontal solid lines. The point (I, v) moves horizontally to the right if $I' > 0$ and to the left if $I' < 0$. Upon reaching the end of either line, (I, v) immediately jumps vertically to the corresponding point on the other line

$E_0 = (1, 0)$. The subsystem with isolation rate v_i has an endemic equilibrium

$$E_i = (S_i^*, I_i^*), \quad i = 1, 2 \tag{7}$$

if $\mathcal{R}_{0i} > 1$, where

$$S_i^* = \frac{\delta + v_i}{\beta - \sigma(\delta + v_i)}, \quad I_i^* = \frac{\mu(1 - S_i^*)(1 + \sigma S_i^*)}{\beta S_i^*} \text{ and } \mathcal{R}_{0i} = \frac{\beta}{(1 + \sigma)(\delta + v_i)}. \tag{8}$$

The two-threshold policy can be represented using a non-ideal relay operator (commonly known as a rectangular hysteresis loop or a lazy switch) (Visintin 1994). To mathematically characterize this hysteresis loop, we introduce the following function space:

(*i*) $BV(0, T)$: the Banach space of functions from $[0, T]$ to $\mathbb{R}_+$ with finite total variation;
(*ii*) $C_r([0, T])$: the linear space of functions that are right-continuous on $[0, T]$.

For any threshold pair $k := (k_*, k_{**})$ with $0 \le k_* < k_{**} \le 1$, we introduce the hysteresis operator

$$w_k : C([0, T]) \times \{0, 1\} \to BV(0, T) \cap C_r([0, T]).$$

More precisely, for any $I(t) \in C([0, T])$ and an initial data $w_k(0) = w_{k0}$ satisfying

$$w_{k0} \begin{cases} = 0, & \text{if } I(0) \le k_*, \\ \in \{0, 1\}, & \text{if } k_* < I(0) < k_{**}, \\ = 1, & \text{if } I(0) \ge k_{**}, \end{cases} \tag{9}$$

and setting $W_t = \{\bar{t} \in (0,t] | I(\bar{t}) = k_* \text{ or } k_{**}\}$, the value of the non-ideal relay operator at time $t > 0$ is

$$w_k(t) = \begin{cases} 0, & \text{if } W_t \neq \emptyset \text{ and } I(\max W_t) = k_*, \\ w_k(0), & \text{if } W_t = \emptyset, \\ 1, & \text{if } W_t \neq \emptyset \text{ and } I(\max W_t) = k_{**}. \end{cases} \tag{10}$$

The relation (10) can be expressed using the operator

$$w_k(t) = (\mathscr{F}_k[w_{k0}]I)(t), \quad t \geq 0. \tag{11}$$

From (10), it follows that the function $w_k(t)$ satisfies the constraint

$$w_k(t) = 1 \text{ whenever } I(t) \geq k_{**}, \quad w_k(t) = 0 \text{ whenever } I(t) \leq k_* \tag{12}$$

for all $t \geq 0$. Moreover, for any $I(t) \in C([0,T])$, the numbers of oscillations between k_* and k_{**} are necessarily finite due to the uniform continuity of $I(t)$. Consequently, $w_k(t)$ switches between 0 and 1 only a finite number of times within any finite interval (Brokate and Sprekels 1996). By combining (10) and (11), the evolution of the isolation rate v can thus be characterized by

$$v(t) = v_1 + (v_2 - v_1)(\mathscr{F}_k[w_{k0}]I)(t), \quad t \geq 0. \tag{13}$$

For the switched system (2), (13) with $\sigma = 0$ and $\mathcal{R}_{01} > 1 > \mathcal{R}_{02}$, Wang and Xiao (2025) demonstrated through theoretical analysis and numerical simulations that any trajectory of this system converges either to an equilibrium of subsystems or to a switch-induced periodic orbit. The specific outcome depends on the threshold levels k_* and k_{**}. In the case of a periodic orbit, the $I-$value oscillates between the threshold levels k_* and k_{**}, as well as the input-output pair $(I(t), v(t))$ evolves counterclockwise along the hysteresis loop illustrated in Fig. 1.

Moreover, the two-threshold strategy is able to suppress the number of infected individuals below the upper threshold k_{**} during the evolution of an infectious disease. For the complementary case where $\mathcal{R}_{01} > \mathcal{R}_{02} > 1$, we can draw the following conclusions based on the concept of real and virtual equilibra, as well as the stability properties of each subsystem, as discussed in Wang and Xiao (2025).

Proposition 1 *Assume that $\mathcal{R}_{01} > \mathcal{R}_{02} > 1$ holds, then switched model (2) with (13) has*

(i) no real equilibrium if $I_2^* < k_* < k_{**} < I_1^*$;
(ii) one real equilibrium E_1 if $I_2^* < k_*$ and $I_1^* < k_{**}$;
(iii) one real equilibrium E_2 if $k_* < I_2^*$ and $k_{**} < I_1^*$;
(iv) two real equilibra E_1 and E_2 if $k_* < I_2^* < I_1^* < k_{**}$.

Moreover, each real equilibrium E_i is at least locally asymptotically stable if $v(0) = v_i$ in the hysteresis region, where $i = 1, 2$.

2.2 The switched system with multiple two-threshold

We note that the switched system (2) with the non-ideal relay operator (13) are used to model isolation as an on-off switching machanism with upper and lower infection thresholds:

(i) if $I(t) \geq k_{**}$, then $v(t) = v_2$ (strict isolation);
(ii) if $I(t) \leq k_{*}$, then $v(t) = v_1$ (relaxed isolation);
(iii) in between k_* and k_{**}, $v(t)$ retains its previous state (hysteresis).

However, this switching rule has some limitations: it oversimplifies isolation policy responses (which are gradual in reality), cannot capture multiple levels of intervention, and fails to incorporate distributed memory effects, where past infection levels influence future decisions. To address these issues, we transition to a discrete Preisach operator, which generalizes hysteresis behavior by incorporating multiple relay elements with distinct threshold pairs. This allows for a more adaptive isolation strategy, where control intensity is adjusted dynamically in response to disease spread. Therefore, we introduce multiple isolation intensities (numbered $i = 1, \cdots, n$), each modifying the isolation coefficient by a specific increment Δv_i. Each isolation strategy follows a rectangular hysteresis loop (13) (see Fig. 1) and is associated with a unique threshold pair $k^i = (k^i_*, k^i_{**})$. Based on these assumptions, the isolation intensity of model (2) is given by

$$v(t) = v_1 + (v_2 - v_1) \sum_{i=1}^{n} p_i \cdot (\mathscr{F}^i_k[w_{k0}]I)(t), \tag{14}$$

where $0 \leq v_1 < v_2$ represent the minimum and maximum values, respectively, that can be implemented by health authorities as control measures, and

$$p_i = \frac{\Delta v_i}{\sum_{j=1}^{n} \Delta v_j}. \tag{15}$$

Therefore, the isolation rate v changes its value at multiple two-threshold $k^i = (k^i_*, k^i_{**})$, $i = 1, 2, \cdots, n$. The operator in (14), involving a discrete set of multiple thresholds, is known as the discrete Preisach model. The thresholds k^i may be organized in a variety of configurations, including non-overlapping thresholds or adjacent, intersecting pairs, as illustrated in Fig. 2, among other possibilities. The number of real and virtual equilibria, as well as the orbit patterns exhibited by model (2), vary according to the specific threshold configurations. For instance, Fig. 3 with $n = 3$ illustrates the input-output relationship associated with the threshold pair combinations depicted in Fig. 2(b). As shown in Fig. 3(a), the trajectory undergoes four switching events. In conjunction with Fig. 3(b), the input-output dynamics ultimately converges to the equilibrium $A = (0.042, 0.19)$, highlighted by a red star. Owing to the complexity introduced by this variability, we shall deeply and theoretically investigate system (2) with continuous Preisach operator, while system (2) with the discrete Preisach operator is illustrated primarily through numerical simulations in Sect. 4.

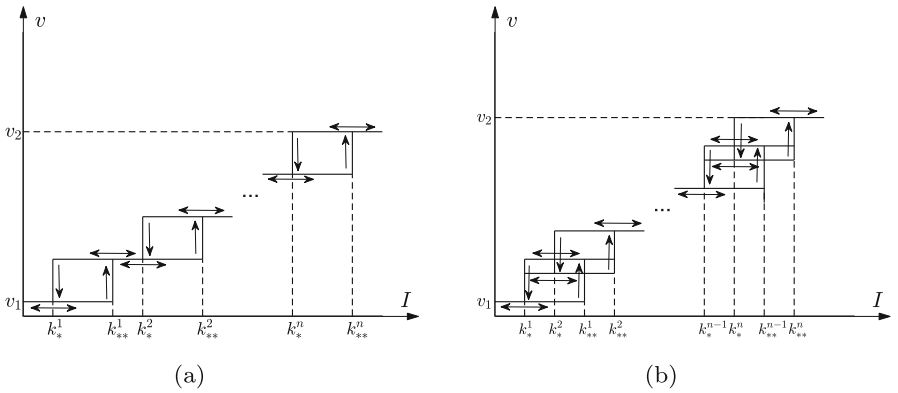


Fig. 2 Schematic diagrams of a switching rule with n hysteresis loops: (a) non-overlapping thresholds, (b) adjacent pairs of intersecting thresholds

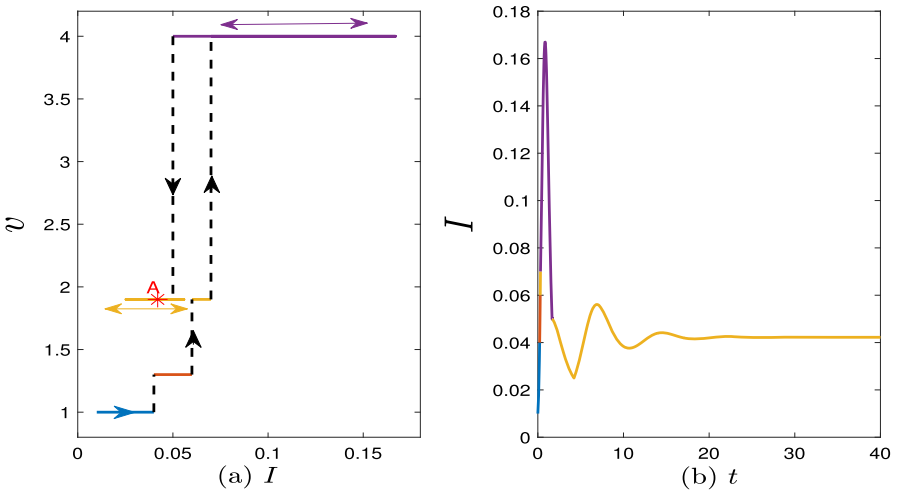


Fig. 3 Panel (a) depicts the input-output relationship of the discrete case (14) for the input $I(t)$ shown in panel (b), incorporating $n = 3$ hysteresis loops. The multiple two-threshold pairs are $(0.02, 0.04)$, $(0.025, 0.06)$ and $(0.05, 0.07)$, with the corresponding weighting parameters p_i in (14) given by $0.1, 0.2$ and 0.7, respectively. The parameters used are $\mu = 0.1, \beta = 10, \sigma = 0.02, \delta = 0.6, v_1 = 1, v_2 = 4$ and $(S_0, I_0) = (0.98, 0.01)$. Moreover, the colored segments indicate the activation of different subsystems

A continuous Preisach operator generalizes the discrete case (14) by integrating over an infinite number of relay elements, each characterized by a unique threshold pair. The isolation rate is now given by

$$v(t) = v_1 + (v_2 - v_1) \iint_{\Theta} p(k)(\mathscr{F}_k[w_{k0}]I)(t)\, dk_1\, dk_2, \qquad t \geq 0, \tag{16}$$

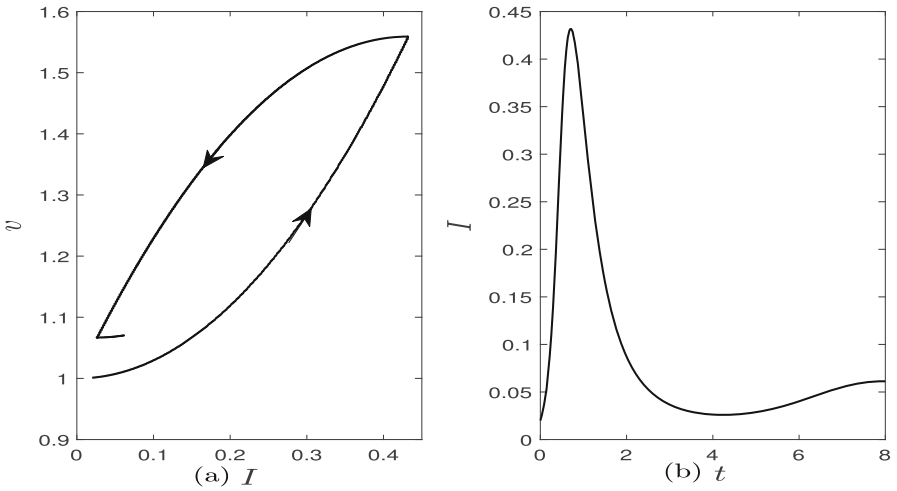


Fig. 4 Panel (a) depicts the input-output relationship of the continuous case (16) for the input $I(t)$ shown in panel (b). A point (I, v) is a turning point if and only if I corresponds to an extreme value of $I(t)$. The parameters used are $\mu = 0.1$, $\beta = 10$, $\sigma = 0.02$, $\delta = 0.6$, $v_1 = 1$, $v_2 = 4$ and $(S_0, I_0) = (0.98, 0.01)$

where $0 \leq v_1 < v_2$ and $0 < p(k) : \Theta \to \mathbb{R}_+$ is a bounded probability density function with

$$\Theta = \{k = (k_1, k_2) \mid 0 \leq k_1 < k_2 \leq 1\}. \tag{17}$$

Hence

$$\iint_{\Theta} p(k)\, dk_1\, dk_2 = 1. \tag{18}$$

This formulation in (16) allows for smooth adjustments to the isolation rate. It overcomes the stepwise nature of the discrete model in (14), and incorporates more realistic memory effects by continuously accounting for past infection levels. Furthermore, $\mathcal{R}_{01}$ denotes the maximal basic reproduction number corresponding to the minimal isolation rate v_1 (subsystem (5)), whereas $\mathcal{R}_{02}$ represents the minimal basic reproduction number associated with the maximal isolation rate v_2 (subsystem (6)). The expressions for $\mathcal{R}_{01}$ and $\mathcal{R}_{02}$ are provided in (8).

Under these assumptions, the evolution of disease in the populations is described by the operator differential model (2), coupled with the adapted control strategy (16). In contrast to Figs. 1 and 2, the relationship between $I(t)$ and $v(t)$ is illustrated in Fig. 4 using an input-output diagram of the real-time control strategy defined by (16). It is observed that at each extreme point of $I(t)$, the input-output pair $(I(t), v(t))$ switches from one branch of $v(t)$ to another. The presence of multiple branches further indicates that the model (2), (16) exhibits a memory effect-meaning that the isolation rate $v(t)$ at time t depends not only on the current infection level $I(t)$ but also on the past values $I(\tau)$ for $\tau \in [0, t)$.

3 Preliminaries

In this section, to facilitate the analysis of the global dynamics of the operator differential model (2) with (16), we first review the properties of the continuous Preisach operator (16), extend the phase space, and then reformulate the system into an autonomous switched form.

3.1 Continuous Preisach operator

We briefly review the definition of the continuous Presach operator (16), as detailed in Visintin (1994); Krasnosel'skii and Pokrovskii (1989). The continuous Preisach operator comprises a set of non-ideal relay operators $\mathscr{F}_k$, each associated with a distinct threshold pair $k \in \Theta = \{k = (k_1, k_2) | \ 0 \leq k_1 < k_2 \leq 1\}$. These operators independently respond to the same continuous input $I(t) : \mathbb{R}_+ \to \mathbb{R}_+$ according to the rule (10). The plane Θ is referred to as the Preisach plane. The output of the Preisach system is a scalar function $v(t) : \mathbb{R}_+ \to \mathbb{R}_+$, defined by (16), where the indicator function

$$w_{k0} = w_k(0) : \ \Theta \to \{0, 1\}$$

denotes the initial state of each operator $\mathscr{F}_k$ for $k \in \Theta$. Additionally, $p(k) : \ \Theta \to \mathbb{R}_+$ is a probability density function that determines the weight distribution of the relay operators w_k. Furthermore, the function $w_k(0)$ is a measurable and satisfies the constraint (9), ensuring compatibility at the initial instant. These conditions guarantee that the integral in (16) is well-defined for any time t and that the output function $v(t)$ remains continuous.

For a fixed moment $t \geq 0$, the function (10), defined over varying k, is regarded as the state function of the Preisach operator, as it characterizes the state of all relay operators at time t. Clearly, this function $w_{k0} = w_k(0) : \ \Theta \to \{0, 1\}$ can be considered an element of the space $L(\Theta; \mathbb{R})$ for any $t \geq 0$. Thus, the relation (10) describes the evolution of $w_k(t)$ in $L(\Theta; \mathbb{R})$ for a given initially compatible input. At each fixed moment t, both the state function $w_k(t)$ and the input $I(t)$ satisfy the compatibility condition (9). Moreover, the evolution of the state function exhibits the semigroup property; i.e.,

$$\text{if } w_k(\tau) = (\mathscr{F}_k[w_{k0}]I)(\tau), \ \text{ then } w_k(t) = (\mathscr{F}_k[w_k(\tau)]I)(t), \ \forall\, k \in \Theta, t \geq \tau \geq 0. \tag{19}$$

For simplicity, we denote the input-output operator given by (16) as

$$v(t) = (\mathscr{P}[w_{k0}]I)(t), \quad \text{for } t \geq 0, \tag{20}$$

where both the initial state w_{k0} and the input $I(t)$ are treated as parameters that satisfy the compatibility condition. The operator's output is given by $v(t)$. According to Krasnosel'skii and Pokrovskii (1989), the Preisach operator (16) is Lipschitz continuous provided that $p(k)$ is bounded. More specifically, for $v^j(t) = (\mathscr{P}[w^j_{k0}]I^j)(t)$ and

$0 \leq I^j(t) \leq 1$ where $j = 1, 2, t \geq 0$, it follows that

$$||v^1(t) - v^2(t)||_{C([0,\tau];\mathbb{R})} \leq l \left(||w_{k0}^1 - w_{k0}^2||_{L(\Theta;\mathbb{R})} + ||I^1(t) - I^2(t)||_{C([0,\tau];\mathbb{R})} \right) \tag{21}$$

for any $\tau \geq 0$, where the Lipschitz constant is given by

$$l := (v_2 - v_1) \sup_{k \in \Theta} p(k).$$

3.2 The extended phase space

Denote the phase space of model (2) with (16) as

$$\Pi = \{(S_0, I_0, w_{k0}) | (S_0, I_0) \in \Omega, w_{k0} = w_0(k) : \Theta \to \{0, 1\}\},$$

where w_{k0} is compatible with I_0. From the global Lipschitz continuous (21), it follows that model (2) with (16) admits a unique local solution for a given initial state w_{k0} and initial condition $(S(0), I(0)) = (S_0, I_0)$ Leonov et al. (2017). Moreover, the trajectory $(S(t), I(t), w_k(t))$ remains within Π for any $t \geq 0$. Due to the positive invariance of Ω, all trajectories can be extended indefinitely along the positive time axis $t \to +\infty$. By the property (19), the projected trajectory in Ω induces a continuous semiflow in the phase space Π, which is endowed with a norm through embedding it into $\mathbb{R}_+^2 \times L(\Theta; \mathbb{R})$. This naturally extends the classical notions of local and global stability for equilibria and periodic solutions in the Lyapunov sense. Specifically speaking, an equilibrium in this system corresponds to a triple $(S_0, I_0, w_{k0}) \in \Pi$, while a periodic orbit is represented by a periodic function $(S(t), I(t), w_k(t)) : \mathbb{R} \times \Theta \to \Pi$, where the function $w_k(t) = w(t; k)$ is defined by (11). At equilibrium, the isolation rate given by (16) remains constant. However, for a periodic orbit, both $v(t)$ and the state function $w_k(t)$ oscillate periodically, synchronized with the periodic variations of $S(t)$ and $I(t)$.

3.3 The autonomous switched system

To analyze the dynamics of the epidemic model (2) with a continuous Preisach operator (16), we transform it into an autonomous form. A fundamental property of hysteresis operators is rate independence, meaning the input-output remains unchanged for any increasing time homeomorphism (Krasnosel'skii and Pokrovskii 1989). More precisely, the inputs $I(t)$ and $I(\zeta(t))$ generate idential input-output graphs (see Fig. 4(a)) for any increasing time transformation $\zeta(t) : \mathbb{R}_+ \to \mathbb{R}_+$. Consequently, at any time t, the value of $w_k(t)$ depends solely on the range of the restriction $I : [0, t] \to \mathbb{R}_+$ and the order in which those values have been attained. For an initial state $w_0 = w_{k0} : \Theta \to \{0, 1\}$, there exists a continuous function $v_{w_0} : \mathbb{R}_+ \to \mathbb{R}_+$ such that the Preisach model (20) can be rewritten as

$$v(t) = v_{w_0}(I(t)), \quad t \geq 0,$$

where any monotone input $I(t) : \mathbb{R}_+ \to \mathbb{R}_+$ is compatible with the initial state w_0. The output v is then defined for piecewise monotone continuous inputs via the semigroup property (19), and subsequently extended to arbitrary continuous inputs by continuity (Krasnosel'skii and Pokrovskii 1989). Moreover, the function $v_{w_0}(I(t))$ is referred to as a branch of the Preisach operator, implying that the initial state function $w_0 = w_{k0}$ parameterizes all possible branches of the Preisach operator. Since the probability density function $p = p(k)$ is assumed to be positive, it follows that every branch $v_{w_0}(I)$ is an increasing function of I over the interval $[0, 1]$.

Based on the above analysis, when the trajectory component $I(t)$ of system (2) with (16) is monotone over the interval $t \in [t_i, t_{i+1}]$, the pair $(S(t), I(t))$ satisfies the following system

$$\begin{aligned} \frac{dS}{dt} &= \mu - \frac{\beta SI}{1+\sigma S} - \mu S, \\ \frac{dI}{dt} &= \frac{\beta SI}{1+\sigma S} - \delta I - v(I)I. \end{aligned} \tag{22}$$

with the isolation rate given by

$$v(I) = v_{w_i}(I), \tag{23}$$

where $w_i = w(t_i)$. This system (22) is referred to as a branch of the operator-differential model (2) with (16), and the state function $w_i = w_{ki}$ serves as a parameter for the family of models (22)-(23). Consequently, the dynamics of model (2) with (16) can be equivalently described as the switching dynamics of model (22)-(23), where transitions between branches occur precisely at times t_i when a solution of (22)-(23) satisfies $I'(t_i) = 0$, i.e.,

$$\frac{\beta S(t_i)}{1+\sigma S(t_i)} = \delta + v_{w_i}(I(t_i)).$$

Throughout this work, the two-dimensional projection $(S(t), I(t))$ of the full state $(S(t), I(t), w(t))$ is also referred to as a solution of model (2) with (16), provided no confusion arises.

4 Main results

In this section, we investigate the set of equilibria and the global stability of system (2) with (16). Additionally, numerical simulations reveal intriguing phenomena in system (2) with the discrete Preisach operator (14), highlighting both its distinctions from and connections to the continuous operator case (16).

As discussed in Sect. 3.2, solutions of model (2) with the continuous Preisach operator (16) evolve within the extended phase space Π, an infinite-dimensional space consisting of triplets (S, I, ω_k). Here the function $\omega_k = \omega(k) : \Theta \ni (k_1, k_2) \to \{0, 1\}$ describes the state values of all relay elements v_k at a given time.

Let us first examine equilibrium states of system (2) with (16). At equilibrium, the solution components S, I, ω_k and the isolation rate v remain constant, with v related

to the function $\omega_k = \omega(k) : \Theta \hookrightarrow \{0, 1\}$ by the equation

$$v = v_1 + (v_2 - v_1) \iint_{\Theta} p(k)\omega_k \, dk_1 \, dk_2. \tag{24}$$

Given assumption (18) and the compatibility constraint (12), the inclusion $k \in \Theta$ ensures that all relays are in the state $w_k = 0$ when $I = 0$. Consequently, system (2) with (16) possesses a unique infection-free equilibrium $E_0 = (1, 0)$, where $\omega_k = \omega(k)$ is the identical zero across Θ, and the isolation rate is $v = v_1$ as given by (24).

On the other hand, it can be shown that if $\mathcal{R}_{01} > \mathcal{R}_{02} > 1$ (as defined in (8)), then system (2) with (16) admits a connected continuum of endemic equilibria

$$E^*_\kappa = (S^*_\kappa, I^*_\kappa) = \left(\frac{\delta + v_\kappa}{\beta - \sigma(\delta + v_\kappa)}, \frac{\mu(1 - S^*_\kappa)(1 + \sigma S^*_\kappa)}{\beta S^*_\kappa} \right), \quad 0 \le \kappa \le 1, \tag{25}$$

each characterized by distinct proportions of the susceptible and infected populations, as well as different isolation rates v_κ. Specifically, we have the following conclusion, with the detailed proof provided in Appendix A.

Theorem 1 *Assuming $\mathcal{R}_{01} > \mathcal{R}_{02} > 1$, the equilibria in (25) form a continuous curve $\widehat{E^*_0 E^*_1}$ in the (S, I)-plane, with E_1 and E_2 as its endpoints.*

As stated in Sect. 3.2, the extended phase space Π of model (2) with (16) is embedded in $\mathbb{R}^2_+ \times L(\Pi; \mathbb{R})$ and is equipped with the corresponding metric. Furthermore, the local and global stability of model (2) with (16) are determined using the standard method. We now analyze the global stability of model (2) with (16) in the following positively invariant set

$$\Pi_0 = \{(S, I, w_k) \in \Pi \mid S > 0, I > 0, S + I \le 1\}.$$

We present the global dynamics results for model (2) with (16) under the conditions $\mathcal{R}_{02} < 1$ and $\mathcal{R}_{02} > 1$, respectively.

Theorem 2 *For model (2), (16) with initial conditions in the positively invariant set Π_0 and $\mathcal{R}_{02} < 1$, the following conclusions hold:*

(*i*) *If $\mathcal{R}_{01} < 1$, the disease-free equilibrium E_0 is globally asymptotically stable.*
(*ii*) *If $\mathcal{R}_{01} > 1$, the disease is uniformly persistent, meaning there exists $\xi > 0$ such that for any initial conditions $S(0) \ge 0$, $I(0) > 0$, the solution of model (2) with (16) satisfies $\liminf_{t \to +\infty} I(t) \ge \xi$.*

Theorem 3 *For model (2), (16) with initial conditions in Π_0 and $\mathcal{R}_{02} > 1$, the following conclusions hold:*

(*i*) *Any trajectory that intersects the nullcline $I' = 0$ (i.e., the curve $\beta S = (1 + \sigma S)(\delta + v(I))$) only finitely many times, will ultimately converge to an endemic equilibrium E^*_κ for some $\kappa \in [0, 1]$.*

(*ii*) *For any trajectory with infinitely many switching events, there exists* $\epsilon \in (0, \mathcal{R}_{01} - 1)$ *such that* $1 + \epsilon \leq \mathcal{R}_{02} < \mathcal{R}_{01}$, *ensuring that the connected continuum of endemic equilibria* E_κ^* *is globally asymptotically stable in* Π_0. *Furthermore, any trajectory converges to an endemic equilibrium* E_κ^* *for some* $\kappa \in [0, 1]$.

The detailed proofs of the above theorems are presented in Appendices B and C. Here, we briefly outline the proof strategies for Theorems 1-3. In Theorem 1, the distribution of equilibria E_κ^* is obtained by analyzing the algebraic equation $h_\kappa(I) = 0$ satisfied by equilibrium states, together with the monotonicity of $h_\kappa(I)$ (33) with respect to I and k. In Theorem 2, the corresponding dynamical behavior is derived using the comparison principle and the persistence theory of semiflows. In Theorem 3, for each branch of the Preisach operator, we construct a Lyapunov function $V_i(S, I)$ of the form (35). By analyzing the increment $\Delta \bar{V}_i$ (38) of the Lyapunov function along trajectories of system (2) with (16) between adjacent switching events, together with the change $\Delta \hat{V}_i$ (45) across different branches at switching points, we establish the global stability of the set of equilibrium states (25) of the system.

To illustrate how the solution of system (2) with (16) looks like, we plot the phase portrait with various initial conditions, shown in Fig. 5. It shows some solutions of the switched system (2) with (16) under a uniform density distribution $p(k) = 2$. The initial conditions introduce a small fraction of infected individuals ($I_0 = 0.01$) into susceptible populations of varying sizes ($S_0 = 0.98, 0.88, 0.78, 0.68$), representing the early stages of an epidemic. According to Theorem 3, these trajectories converge to different equilibria E_κ^*, where $\kappa \in [0, 1]$. The endpoints of the continuum of endemic equilibria E_κ^*, defined by (25), are marked by red stars. Our simulation results further suggest that a population with a higher initial proportion of susceptible individuals exhibits two key characteristics:

(*i*) a higher initial peak of infected individuals, and
(*ii*) eventual convergence to an equilibrium with a greater proportion of susceptible individuals S_κ^* and a lower proportion of infected population I_κ^*. At this stage, the original system (1) with (16) has a lower proportion of quarantined population Q_κ^* and recovered population R_κ^*, where

$$Q_\kappa^* = \frac{\upsilon_\kappa I_\kappa^*}{\gamma_2 + \mu} \quad \text{and} \quad R_\kappa^* = \frac{\gamma_1 I_\kappa^* + \gamma_2 Q_\kappa^*}{\mu}.$$

This demonstrates that, although the connected continuum of endemic equilibria E_κ^* is globally asymptotically stable, the specific equilibrium approached by each trajectory depends on the initial conditions.

To compare the trajectories of switched system with discrete and continuous Preisach operator, we plot the phase portrait with different values of parameter n (representing n hysteresis loops). Fig. 6 illustrates simulations of several solutions to the switched system (2) incorporating the discrete Preisach operator (14), with identical initial conditions ($S_0 = 0.98$, $I_0 = 0.01$) and varying values of $n = 2, 4, 6, 8$. The results demonstrate that as n increases, the trajectories progressively converge to the orbit of the system with the continuous Preisach operator (16) under the same initial

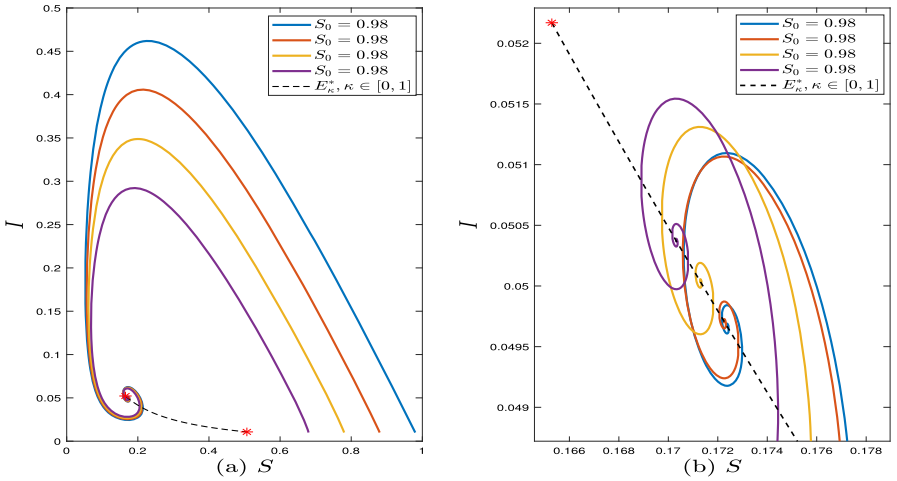


Fig. 5 (a) The trajectories of the switched system (2), (16) with $I_0 = 0.01$ and varying values of $S_0 = 0.98, 0.88, 0.78, 0.68$. The Preisach operator (16) is applied with a uniform density function $p(k) = 2$, while all other parameters remain the same as in Figure 4. The endpoints of the continuum of endemic equilibria E^*_κ are marked by red stars. (b) A magnified view of a localized region in panel (a)

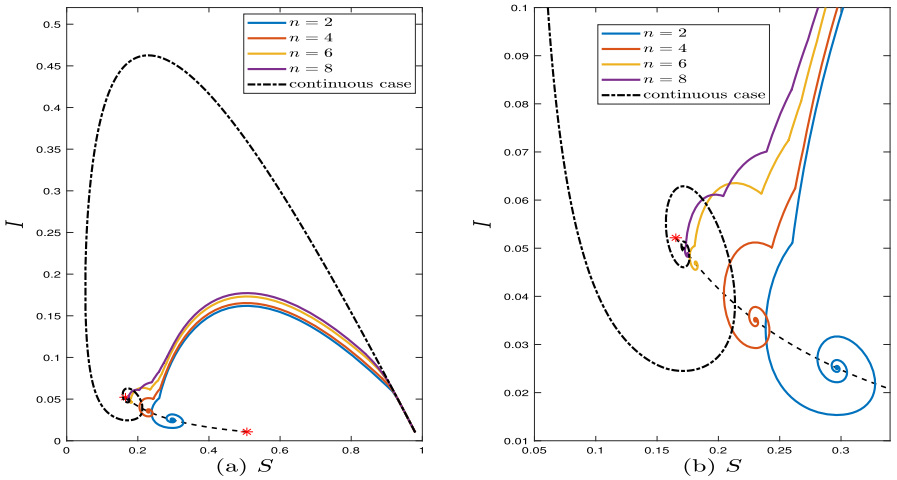


Fig. 6 (a) The trajectories of the switched system (2) with respect to the discrete case (14) ($n = 2, 4, 6, 8$) and the continuous case (16). Here the initial condition $(S(0), I(0)) = (0.98, 0.01)$, while all other parameters remain the same as in Fig. 4. (b) A magnified view of a localized region in panel (a)

conditions. Moreover, greater heterogeneity (greater values of n) leads to higher peaks of infected individuals during the epidemic and more severe disease prevalence in the long term.

It is interesting to note that the switched system (2) with the discrete Preisach operator (14) consists of at most 2^n subsystems, each corresponding to one of 2^n stable endemic equilibria. The exact number of equilibria depends on the composition of the n hysteresis loops (see Fig. 2), the weights p_i in (15), and the parameters of

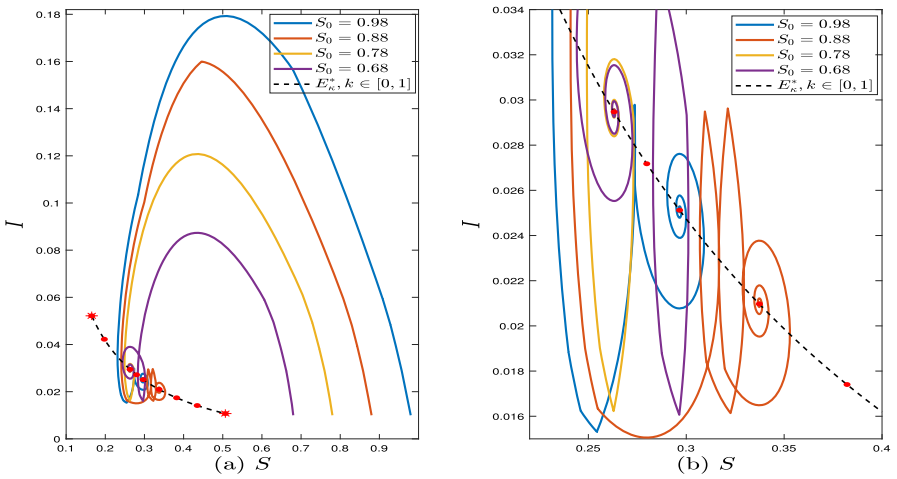


Fig. 7 (a) The trajectories of the switched system (2) with (14) are shown for $I_0 = 0.01$ and varying values of $S_0 = 0.98, 0.88, 0.78, 0.68$. The discrete Preisach operator (14), incorporating $n = 6$ hysteresis loops, is applied. The switched system (2) exhibits 9 stable equilibria (marked as red dots), all of which lie on the curve E^*_κ for $\kappa \in [0, 1]$. (b) A magnified view of a localized region from panel (a) is presented. The multiple two-threshold pairs are (0.015, 0.05), (0.014, 0.04), (0.016, 0.03), (0.018, 0.03), (0.026, 0.062) and (0.1, 0.16), with the corresponding weighting parameters p_i in (14) given by 0.25, 0.1, 0.17, 0.13, 0.15 and 0.2, respectively. All other parameters remain consistent with those in Fig. 4

system (2). Here, we shall show different composition of the 6 hysteresis loops induce the quite different number of stable endemic equilibria. In particular, Fig. 7, shows that for a discrete Preisach operator with six hysteresis loops, there are 9 equilibria through numerical computation. We observe that trajectories with a higher proportion of susceptibles experience greater peak infections. This behavior is consistent with the characterization of system (2) incorporating the continuous Preisach operator (16). Figure 8 presents sample trajectories for system (2) with (14) under the same conditions and with the same number of hysteresis loops, but with six distinct two-thresholds pairs. However, in this case, this model exhibits 23 stable equilibria, represented by red dots. Moreover, the equilibria of system (2) with a discrete Preisach operator are located within the connected continuum of endemic equilibria $\widehat{E^*_0 E^*_1}$ of system (2) with the corresponding continuous Preisach operator.

Furthermore, it is worth that system (2) with (14) can exhibit multistability, characterized by multiple equilibria and periodic solutions. Specifically, Fig. 9 demonstrates the existence of 18 equilibria along with several periodic solutions, corresponding to the same number of threshold pairs but with different values in Fig. 8. This behavior is consistent with the findings of system (2) with the non-ideal relay operator (13) in Wang and Xiao (2025), where a bistability phenomenon arises, consisting of an equilibrium of the subsystems and a switch-induced periodic orbit.

It would be interesting to include numerical simulations to design optimal thresholds (k_* and k_{**}) aligned with practical disease control objectives for non-ideal relay operator. To account for disease transmission losses, implemention costs of control

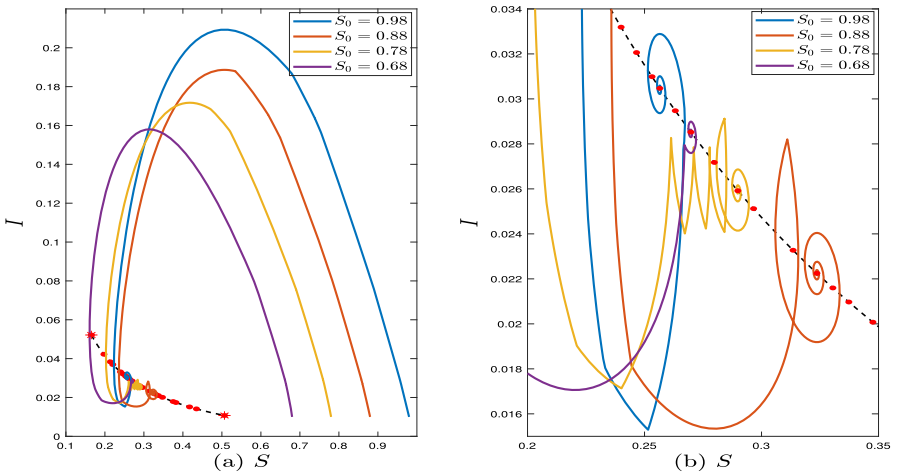


Fig. 8 (a) The trajectories of the switched system (2) with (14) are shown for $I_0 = 0.01$ and varying values of $S_0 = 0.98, 0.88, 0.78, 0.68$. The discrete Preisach operator (14), incorporating $n = 6$ hysteresis loops, is applied. The switched system (2) exhibits 23 stable equilibria (marked as red dots). (b) A magnified view of a localized region from panel (a) is presented. The multiple two-threshold pairs are $(0.015, 0.19)$, $(0.015, 0.17)$, $(0.017, 0.08)$, $(0.018, 0.03)$, $(0.024, 0.0285)$ and $(0.04, 0.16)$. All other parameters remain consistent with those in Fig. 7

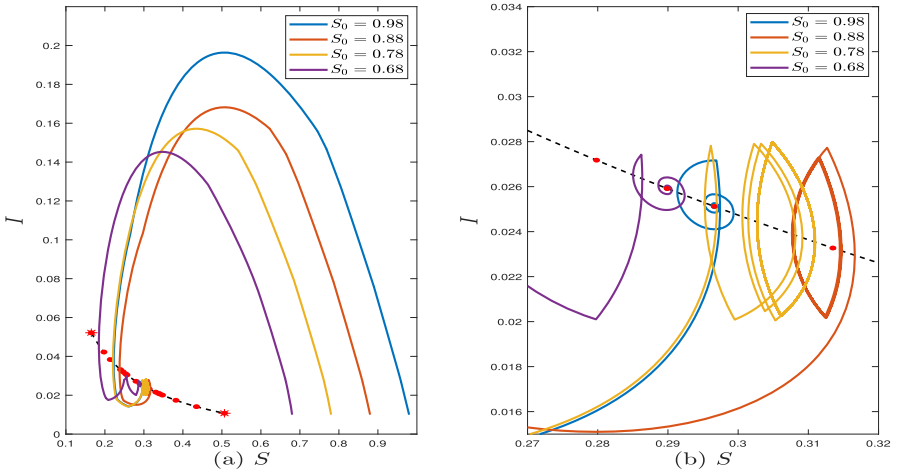


Fig. 9 (a) The trajectories of the switched system (2) with (14) are shown for $I_0 = 0.01$ and varying values of $S_0 = 0.98, 0.88, 0.78, 0.68$. The discrete Preisach operator (14), incorporating $n = 6$ hysteresis loops, is applied. The switched system (2) exhibits 18 equilibria (marked as red dots) and some periodic solutions. (b) A magnified view of a localized region from panel (a) is presented. The multiple two-threshold pairs are $(0.012, 0.15)$, $(0.014, 0.13)$, $(0.017, 0.08)$, $(0.018, 0.03)$, $(0.02, 0.028)$ and $(0.1, 0.16)$. All other parameters remain consistent with those in Fig. 7

measures, and a reasonable hysteresis structure, we introduce the following objective functional

$$J_\alpha(k) = \int_0^T [AI(t;k) + Bv_k^2(I(t))]dt + C[(k_{**} - k_*) - k_0]^2, \tag{26}$$

where $A > 0$, $B > 0$ and $C > 0$ are weight parameters, and k_0 denotes a prescribed threshold window determined from historical experience or operational constraints. The first term of (26) represents the cumulative disease burden over the entire period $[0, T]$, minimizing it aims to reduce the persistence and overall prevalence of infection. The second term captures the cost of implementing intervention measures. In particular, the quadratic form $v_k^2(I(t))$ penalizes high-intensity interventions, thereby discouraging prolonged periods of stringent control. The third term enforces that the optimal thresholds k_*, k_{**} with $k_{**} - k_*$ being close to the desired hysteresis width k_0. A threshold window that is too wide may lead to sluggish system response, while a window that is too narrow causes excessive switching when infection levels fluctuate near the thresholds (Wang and Xiao 2025; Wang et al. 2026). The optimal threshold design problem can then be formulated as

$$\min_{(k_*,k_{**})\in\Gamma} J_\alpha(k),$$

where the feasible set is defined by

$$\Gamma := \{(k_*, k_{**}) \in \mathbb{R}_+^2 \mid 0 \le k_* < k_{**} \le \bar{I}\},$$

with $\bar{I} > 0$ a prescribed upper bound. We numerically solved the optimal problem and obtained the optimal threshold pair $(k_*, k_{**}) \approx (0.078, 0.304)$, as illustrated in Fig. 10. Note that Fig. 10(a) shows that the objective functional $J_\alpha(k)$ is discontinuous in the (k_*, k_{**}) plane. This discontinuity arises because for k_{**} greater than a critical level k_{**}^{th} (here, $k_{**}^{th} = 0.355$), the system with a non-ideal relay operator always follows subsystem (5), resulting in no switching, whereas for k_{**} less than the critical level k_{**}^{th} ($k_{**} < k_{**}^{th}$), the system switches between subsystems (5) and (6). Consequently, near $k_{**} = k_{**}^{th}$, the value of $J_\alpha(k)$ exhibits a jump.

Finally, we describe the basin of attraction corresponding to each stable state when multistability occurs in a system with a non-ideal relay operator. When the equilibrium $E_i (i = 1, 2)$ (7) of the subsystem of system (2) lies within the hysteresis region (i.e., $k_* < I_i^* < k_{**}$), and $v(0) = v_i$ for $k_* < I(0) < k_{**}$, the system frequently exhibits multistability. In such case, the basin of attraction of the steady state lies inside the hysteresis region (see Fig. 11(b)), while the remaining region typically corresponds to the basin of attraction of a periodic solution. To illustrate this, we present specific numerical simulation results. We fix $k_* = 0.008$ and choose the threshold window $h := k_{**} - k_*$ as a bifurcation parameter to identify the range of threshold values at which multistability occurs. As can be seen from Fig. 11(a), when $h \in (0.0445, 0.0785)$, the system exhibits bistability, characterized by the coexistence of an equilibrium and a periodic orbit. In this regime, the shaded region denotes the basin of attraction of the equilibrium, while the complementary region corresponds to that of the periodic solution, as shown in Fig. 11(b). For the discrete Preisach operator,

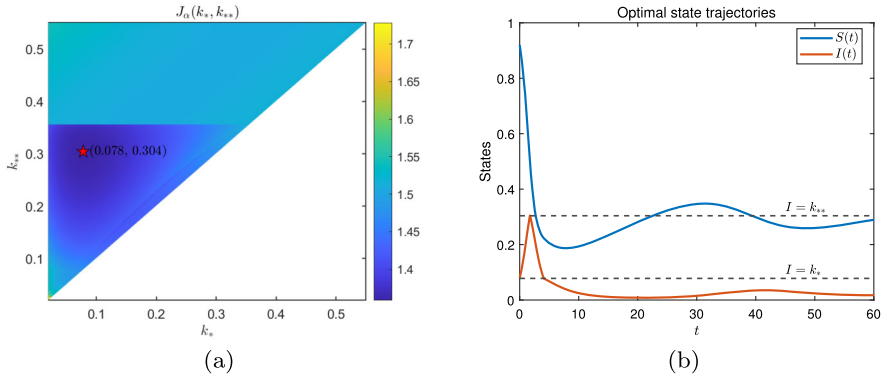


Fig. 10 (a) Numerical results of system (2) with a non-ideal relay operator for the control objective $\min_{(k_*,k_{**})\in\Gamma} J_\alpha(k)$. The optimal threshold pair is found to be $(k_*, k_{**}) \approx (0.078, 0.304)$, indicated by a star. (b) The evolution of state trajectory over time under optimal threshold pair. The parameters used are $\mu = 0.02, \beta = 2.4, \sigma = 0.35, \delta = 0.55, v_1 = 0.08, v_2 = 0.7, A = 0.58, B = 0.12, C = 0.3, k_0 = 0.18, \bar{I} = 0.55$, with initial condition $(S_0, I_0) = (0.92, 0.08)$

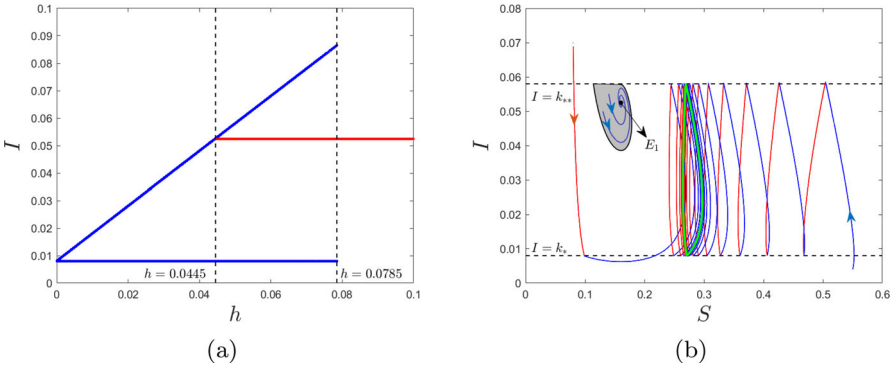


Fig. 11 (a) Bifurcation diagram of system (2) with a non-ideal relay operator. The threshold window h serves as the bifurcation parameter, with $k_* = 0.008$ and $v_2 = 8$. The blue curve represents the maximum and minimum values of the periodic solution, while the red curve denotes the equilibrium value E_1. Between the two dashed lines (i.e., $h \in (0.0445, 0.0785)$), a bistability phenomenon is observed, where both the periodic solution and the equilibrium E_1 coexist. (b) Bistability phenomenon of system (2) with a non-ideal relay operator for $h = 0.05$. The shaded region denotes the basin of attraction of the equilibrium, while the white region corresponds to that of the periodic solution. The red curve represents the solution corresponding to high isolation intensity v_2, the blue curve corresponds to low isolation intensity v_1, and the green curve denotes the periodic solution. The remaining parameter values are the same as those in Fig. 4

the structure of stable states, including the number of equilibria, periodic solutions, and their corresponding attractor basins, is highly intricate. This complexity arises from the multitude of possible combinations of n hysteresis loops. In contrast, for the continuous Preisach operator, when the condition $\mathcal{R}_{01} > \mathcal{R}_{02} > 1$ is satisfied, the continuum of equilibria forms a singular line, and the attractor basin associated with this line spans the entire feasible domain.

5 Discussion

Infectious disease models play a crucial role in analyzing epidemic dynamics and evaluating the effectiveness of control strategies. Traditional epidemic models typically assume homogeneous control measures, but in reality, prevention and control strategies vary significantly due to social, economic, and governmental influences. As a starting point, we consider an SIQR model with a lazy-switch mechanism (13), where quarantine/isolation strategies are activated once the number of infected individuals exceeds a critical threshold and are suspended only when it falls below a lower threshold (Wang and Xiao 2025). Building on this foundation, we introduce nonlinear incidence and, more importantly, a heterogeneous isolation rate, which is modeled using the Preisach operator. This operator captures key real-world quarantine dynamics, including:

- (i) Threshold-based decision-making: Quarantine measures activate or lifted based on whether infections surpass or fall below critical levels.
- (ii) Past-dependent isolation policies: When past infection levels were high, control measures may remain strict even when infections decrease.
- (iii) Saturation effects: Limited quarantine capacity leads to nonlinear responses in the implementation of control measures.

By incorporating the Preisach operator, the model introduces a nonlinear, rate-independent hysteresis effect into quarantine dynamics, better reflecting the memory and delayed response observed in real-world epidemic control strategies. Hence, we extend previous studies on SIQR models with non-ideal relay operators, where switching surfaces were fixed straight lines (Wang and Xiao 2025).

It is well known that a typical switched system comprises a finite set of vector fields and a logic rule governing the transitions between them. Notably, such switching mechanisms can induce instability, even when each individual subsystem remains stable (Liberzon and Morse 1999). For example, if system (2) adopts a simple linear connection between v_1 and v_2, i.e.,

$$v(I) = \begin{cases} v_1, & \text{if } I < k_*, \\ v_1 + \dfrac{v_2 - v_1}{k_{**} - k_*}(I - k_*), & \text{if } k_* \le I \le k_{**}, \\ v_2, & \text{if } I > k_{**}, \end{cases} \tag{27}$$

the system becomes piecewise-smooth continuous system with three vector fields (Bernardo et al. 2008; Simpson 2010). In such case, the system's dynamics depend solely on the current number of infected individuals, without memory effects. In contrast, the SIQR model incorporating a Preisach operator involves an infinite family of nonlinear planar vector fields and exhibits memory effects, meaning that the current level of isolation depends not only on the current number of infected individuals but also on the past evolution of the disease. This hysteresis-driven switching results in a continuum of equilibria (25) and multistability, as evidenced by the coexistence of multiple equilibria and periodic solutions shown in Fig. 9. Consequently, the two switching mechanisms generate substantially different dynamics. Within the switched

system framework, the trajectory of model (2) with (16) between successive switching moments follows the integral curve of a globally stable subsystem, characterized by a corresponding Lyapunov function. The Preisach operator dictates the switching rule, governing transitions between subsystems that correspond to different branches of the hysteresis operator. In this work, we generalize the stability analysis to account for dynamically evolving switching surfaces, providing a broader perspective on the impact of hysteresis-driven isolation policies in epidemic control.

The presence of multiple endemic equilibria in an SIQR model with the Preisach operator highlights the complex interplay between past control measures, hysteresis effects, and current infection dynamics. To further explore these dynamics, we analyze the global stability of model (2) with (16). In particular, when $\mathcal{R}_{01} > 1$, the disease is uniformly persistent (Theorem 2) and the connected continuum of endemic equilibria are globally asymptotically stable for $\mathcal{R}_{02} > 1$ under certain codidtions (Theorem 3). This global stability analysis method leverages a family of Lyapunov functions, each corresponding to a different branch of the hysteresis operator, by transforming the system into a switched framework (Di Bernardo et al. 2008).

This finding explains why some communities may stabilize at low infection levels due to strong or proactive interventions, while others, experiencing weaker or delayed responses, remain at a higher endemic state. Our results reveal that the model (2) with the Preisach operator (16) admits a continuum of endemic equilibria, each characterized by distinct proportions of susceptible, infectious, quarantined, and recovered individuals. The existence of multiple endemic equilibria in an SIQR model suggests that different population groups adopt varying quarantine and isolation measures based on past experiences. Specifically, populations that have previously experienced severe infection waves may enforce stricter and longer-lasting control measures, stabilizing at a lower endemic equilibrium. In contrast, populations with a history of mild outbreaks may relax quarantine measures more quickly, leading to a higher endemic equilibrium. This underscores the role of behavioral memory in shaping disease persistence and control effectiveness. These insights are crucial for designing adaptive public health policies that account for hysteresis effects and heterogeneous quarantine compliance, ensuring more effective epidemic control strategies.

It is worth noting that the model we proposed here is a type of SIQR model, but we expect that the approaches employed could be applied more generally, say, SEIQR-type models. The theoretically analysis may becomes increasingly complex for higher dimensions, and the core technique is to analyze the reduced model in a relatively low dimension. In such reduced models, the continuum of equilibria may form a surface rather than a curve. Regarding the different incidence rates, when $\sigma = 0$, system (2) reduces to a model with mass-action incidence. In such case, the derivations of all subsequent theorems remain valid, although the continuum of equilibria becomes a straight line instead of a curve. For system (2) with a non-constant total population and standard incidence, constructing appropriate Lyapunov functions for the different branches of the Preisach operator is generally challenging. Further, note that under the scenario described in Theorem 2 (ii) (i.e., $\mathcal{R}_{02} < 1 < \mathcal{R}_{01}$), some constituent subsystems have the basic reproduction number greater than 1, while others have it less than 1, and consequently the condition does not guarantee global stability of either

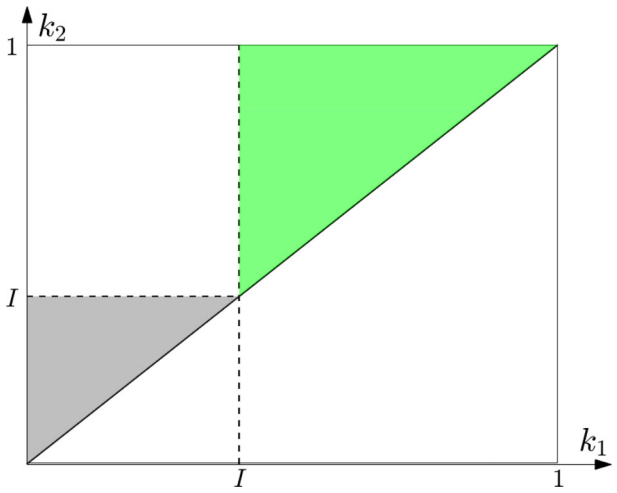


Fig. 12 A schematic diagram illustrating the values of $\omega_k = \omega(k)$ for a given point I within the domain $\Theta = \{k = (k_1, k_2) | \ 0 \le k_1 < k_2 \le 1\}$. Specifically, $\omega_k = 1$ in the shaded region, $\omega_k = 0$ in the green region, and ω_k can be either 0 or 1 in the white region

periodic or equilibrium states. Then we obtained the relatively conclusion, namely, the persistence of the disease.

Appendices

In this section, we present the proofs of Theorems 1–3.

A. Proof of Theorem 1

Proof Denote

$$\bar{v}(I) = v_1 + (v_2 - v_1) \int_0^I dk_2 \int_0^{k_2} p(k)\, dk_1, \tag{28}$$

$$\hat{v}(I) = v_2 - (v_2 - v_1) \int_I^1 dk_2 \int_I^{k_2} p(k)\, dk_1, \tag{29}$$

$$v_\kappa(I) = (1 - \kappa)\bar{v}(I) + \kappa \hat{v}(I), \tag{30}$$

where $\kappa \in [0, 1]$. For a given I, $\bar{v}(I)$ and $\hat{v}(I)$ represent the minimum and maximum values of $v(t)$ in (16), respectively. Both values correspond to the white regions in the domain Θ in Fig. 12, where $\omega_k = 0$ and $\omega_k = 1$, respectively.

We note that both $\bar{v}(I)$ and $\hat{v}(I)$ strictly increase with I. From the normalization condition (18) and the fact that $p(k) > 0$, it follows that

$$\begin{aligned} &\bar{v}(0) = \hat{v}(0) = v_1, \quad \bar{v}(1) = \hat{v}(1) = v_2, \\ &\hat{v}(I) > \bar{v}(I) \ \text{ for } \ I \in (0, 1). \end{aligned} \tag{31}$$

The constraint (9) means that for any endemic equilibrium (S^*, I^*), there exists a $\kappa \in [0, 1]$ such that the isolation rate satisfies $v = v_\kappa(I^*)$. Moreover, S^* and I^* depend on v as given by expression (27). Therefore, (S^*, I^*) is an endemic equilibrium if and only if there exists $\kappa \in [0, 1]$ such that

$$S^* = \frac{\delta + v_\kappa(I^*)}{\beta - \sigma(\delta + v_\kappa(I^*))}, \quad I^* = \frac{\mu(1 - S^*)(1 + \sigma S^*)}{\beta S^*}. \tag{32}$$

Note that the continuous function $v_\kappa(I)$, defined by (30), strictly increases with κ for $I \in (0, 1)$ and is also strictly increasing in I. Hence, the continuous function, $0 \le I, \kappa \le 1$,

$$h_\kappa(I) := \frac{\mu(1 - S)(1 + \sigma S)}{\beta S} - I = \frac{\mu}{\beta}\left(\frac{\beta}{\delta + v_\kappa(I)} - \frac{\sigma}{\frac{\beta}{\delta + v_\kappa(I)} - \sigma} - 1\right) - I, \tag{33}$$

decreases with respect to I and κ. Further, for any $\kappa \in [0, 1]$, the relations

$$\begin{aligned} h_\kappa(0) &= \frac{\mu}{\beta}\left(\frac{\beta}{\delta + v_1} - \frac{\sigma}{\frac{\beta}{\delta + v_1} - \sigma} - 1\right) > 0, \\ h_\kappa(1) &= \frac{\mu}{\beta}\left(\frac{\beta}{\delta + v_2} - \frac{\sigma}{\frac{\beta}{\delta + v_2} - \sigma} - 1\right) - 1 < 0, \end{aligned}$$

which follow from (18) and $\mathcal{R}_{01} > \mathcal{R}_{02} > 1$. This implies that $h_\kappa(I) = 0$ has a unique root $I_\kappa^* \in (0, 1)$ for any given $\kappa \in [0, 1]$. Moreover, by the Implicit Function Theorem, this root decreases continuously with κ. It follows from (32) that the endemic equilibria E_κ^* for $0 \le \kappa \le 1$ form a non-degenerate curve $\widehat{E_0^* E_1^*}$ in the $(S, I)-$plane. From (30)-(31), we obtain $v_1 \le v_\kappa(I) \le v_2$. In particular, the $I-$value of the endpoints of the curve $\widehat{E_0^* E_1^*}$ correspond to the zeros I_i^* of $h_i(I) = 0$ for $i = 0, 1$, as illustrated in Fig. 13. Furthermore, by combining (7) and (32), we conclude that E_0^* and E_1^* are the curve $\widehat{E_0^* E_1^*}$ endpoints. □

B. Proof of Theorem 2

Proof If $\mathcal{R}_{01} < 1$, the second equation in (2) gives

$$I' = \frac{\beta S I}{1 + \sigma S} - \delta I - v(t) I \le \left(\frac{\beta}{1 + \sigma} - \delta - v_1\right) I < 0.$$

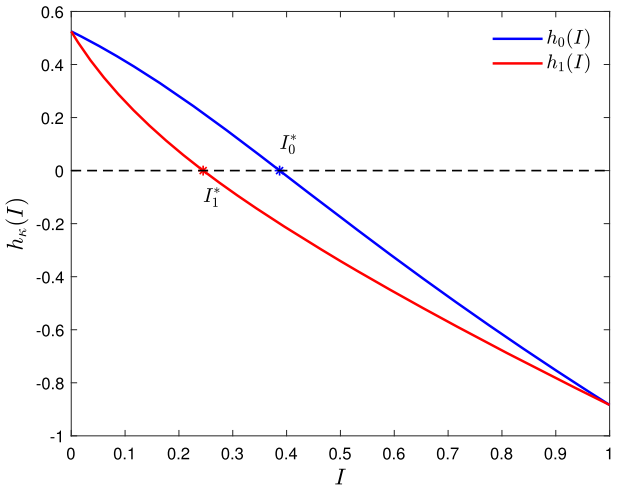


Fig. 13 The interval $[I_1^*, I_0^*]$ represents the projection of the connected continuum of endemic equilibria E_κ^*, given by (25), onto the $I-$axis

This implies that $I(t)$ decreases monotonically to zero. Consequently, every trajectory of (2) converges to the disease-free equilibrium $E_0 = (1, 0)$, establishing conclusion (i).

When $\mathcal{R}_{02} < 1 < \mathcal{R}_{01}$, assume that there exists a solution with $I(t) > 0$ and $\lim_{t\to+\infty} I(t) = 0$. Hence, for any $\epsilon \in (0, 1)$ and sufficiently large t, we obtain

$$I(t) \leq \frac{\epsilon\mu}{\beta(1-\epsilon)}$$

and

$$S'(t) = \mu - \frac{\beta S(t)I(t)}{1 + aS(t)} - \mu S(t) \geq \mu - (\beta I + \mu)S(t).$$

Hence,

$$\liminf_{t\to+\infty} S(t) \geq \frac{\mu}{\mu + \frac{\epsilon\mu}{1-\epsilon}} = 1 - \epsilon$$

for any $\epsilon > 0$. On the other hand,

$$S'(t) \leq \mu - \mu S(t),$$

which implies $\limsup S(t) \leq 1$. Hence, we conclude that $\lim_{t\to+\infty} S(t) = 1$. Furthermore, for any $\epsilon > 0$ and sufficiently large t, we have $S(t) > 1 - \epsilon$. The second equation of (2) implies that

$$I' > \left(\frac{\beta(1-\epsilon)}{1 + \sigma(1-\epsilon)} - \delta - v_1\right) I > 0$$

since $v(t) = v_1$ when I is sufficiently small. This contradicts the assumption $\lim_{t\to+\infty} I(t) = 0$, leading to $\limsup_{t\to+\infty} I(t) > 0$.

To complete the proof, we apply the persistence theory of semiflows (Smith and Thieme 2011). For a solution where $I(t) = 0$, we have $S' = \mu - \mu S$, leading to $\lim_{t\to+\infty} S(t) = 1$. Any solution in the subspace $\{(S, I) \in \Omega \mid I = 0\}$ converges to the disease-free equilibrium E_0, which is clearly an acyclic cover of the $\omega-$limit sets of such solutions. By Theorem 8.17 in (Smith and Thieme 2011), it follows from that the disease is uniformly weak persistent, i.e., there is a constant $\xi > 0$ such that $\limsup_{t\to+\infty} I(t) > \xi$ for all trajectories where $I(t) > 0$. Moreover, by Theorem 4.5 in (Smith and Thieme 2011), we conclude that the disease is uniformly persistent, thus establishing conclusion (ii).

□

C. Proof of Theorem 3

Global stability results for the infinite-dimensional switched system (2), (16) with $\mathcal{R}_{01} > \mathcal{R}_{02} > 1$ are established by analyzing a series of Lyapunov functions. Lemmas 1 and 2 specify the form and properties of the Lyapunov function corresponding to each branch of the Preisach operator. Lemmas 3-7 provide estimates of the increment over an entire switching event, while Lemmas 8-10 show that every trajectory of system (2) with (16) converges to an endemic equilibrium E_κ^* for some $\kappa^* \in [0, 1]$.

C.1 Lyapunov function for each branch

Lemma 1 *Model (22) with any branch $v(I) = v_{\omega_i}(I)$ has a unique disease-free equilibrium $(1, 0)$ and a unique endemic equilibrium (S_*, I_*), where*

$$S_* = \frac{\delta + v(I_*)}{\beta - \sigma(\delta + v(I_*))}$$

and I_* satisfies

$$\frac{\delta + v(I)}{\beta - \sigma(\delta + v(I))} = \frac{\mu - \delta I - v(I)I}{\mu}. \tag{34}$$

Moreover, the disease-free equilibrium is unstable, while the endemic equilibrium (S_*, I_*) is globally asymptotically stable in positively invariant set Ω_0.

Proof Denote

$$g(I) = \frac{\delta + v(I)}{\beta - \sigma(\delta + v(I))} + \frac{\delta I + v(I)I - \mu}{\mu}.$$

Due to the assumption $\mathcal{R}_{01} > \mathcal{R}_{02} > 1$ and $v(I)$ is an increasing function, we have

$$g(0) = \frac{\delta + v(0)}{\beta - \sigma(\delta + v(0))} - 1 = \frac{\delta + v_1}{\beta - \sigma(\delta + v_1)} - 1 < 0$$

and

$$g(1) = \frac{\delta + v(1)}{\beta - \sigma(\delta + v(1))} + \frac{\delta + v(1) - \mu}{\mu} = \frac{\delta + v_2}{\beta - \sigma(\delta + v_2)} + \frac{\delta + v_2 - \mu}{\mu} > 0,$$

as well as $g(I)$ is also an increasing function. Therefore, the equation (34) has a unique solution $I_* \in (0, 1)$.

The characteristic equation of model (22) at the point $(1, 0)$ has eigenvalues $\lambda_1 = -\mu$ and $\lambda_2 = (\delta + v_1)(\mathcal{R}_{01} - 1) > 0$, given the assumption $\mathcal{R}_{01} > \mathcal{R}_{02} > 1$. This means that the disease-free equilibrium $(1, 0)$ is unstable.

At the endemic equilibrium (S_*, I_*), The characteristic equation of model (22) is given by

$$\lambda^2 + \left(\mu + v'(I_*)I_* + \frac{\beta I_*}{(1+\sigma S_*)^2}\right)\lambda + \frac{\beta^2 S_* I_*}{(1+\sigma S_*)^3} + v'(I_*)I_*\left(\mu + \frac{\beta I_*}{(1+\sigma S_*)^2}\right) = 0.$$

Since $v(I)$ is increasing, all coefficients of this equation are positive. Consequently, all roots of the characteristic equation have negative real parts, ensuring, the endemic equilibrium (S_*, I_*) is locally asymptotically stable.

We consider the following Lyapunov function

$$\begin{aligned} V(S(t), I(t)) &= \int_{S_*}^{S(t)} \left(1 - \frac{1+\sigma\theta}{1+\sigma S_*}\frac{S_*}{\theta}\right) d\theta + \int_{I_*}^{I(t)} \left(1 - \frac{I_*}{\theta}\right) d\theta \\ &= S(t) - S_* - \int_{S_*}^{S(t)} \left(\frac{1+\sigma\theta}{1+\sigma S_*}\frac{S_*}{\theta}\right) d\theta + I(t) - I_* - I_* \ln \frac{I(t)}{I_*}. \end{aligned} \tag{35}$$

Noting that

$$\mu = \frac{\beta S_* I_*}{1+\sigma S_*} + \mu S_*, \quad \delta = \frac{\beta S_*}{1+\sigma S_*} - v(I_*),$$

and calculating the derivation of $V(S, I)$ along a trajectory of model (22), we obtain

$$\begin{aligned} V' &= \left(1 - \frac{S_*}{S}\frac{1+\sigma S}{1+\sigma S_*}\right)\left(\mu - \frac{\beta SI}{1+\sigma S} - \mu S\right) \\ &\quad + \left(1 - \frac{I_*}{I}\right)\left(\frac{\beta SI}{1+\sigma S} - \delta I - v(I)I\right) \\ &= \left(1 - \frac{S_*}{S}\frac{1+\sigma S}{1+\sigma S_*}\right)\left(\frac{\beta S_* I_*}{1+\sigma S_*} + \mu S_* - \frac{\beta SI}{1+\sigma S} - \mu S\right) \\ &\quad + \left(1 - \frac{I_*}{I}\right)\left(\frac{\beta SI}{1+\sigma S} - v(I)I - \frac{\beta S_*}{1+\sigma S_*}I + v(I_*)I\right) \\ &= -\frac{\mu(S - S_*)^2}{S(1+\sigma S_*)} + \frac{\beta S_* I_*}{1+\sigma S_*}\left(2 - \frac{S_*}{S}\frac{1+\sigma S}{1+\sigma S_*} - \frac{S}{S_*}\frac{1+\sigma S_*}{1+\sigma S}\right) \\ &\quad + (v(I_*) - v(I))(I - I_*). \end{aligned}$$

Since $v(I)$ is an increasing function, we have

$$(v(I_*) - v(I))(I - I_*) \le 0, \quad \text{and} \quad 2 - \frac{S_*}{S}\frac{1+\sigma S}{1+\sigma S_*} - \frac{S}{S_*}\frac{1+\sigma S_*}{1+\sigma S} \le 0.$$

Therefore, we conclude that $V'(S, I) \le 0$, and $V'(S, I) = 0$ if and only if $(S, I) = (S_*, I_*)$. When $(S, I) \ne (S_*, I_*)$,

$$V' \le -\frac{\mu(S - S_*)^2}{S(1+\sigma S_*)} < 0. \tag{36}$$

It follows from Theorem 5.3.1 in (Hale and Lunel 1993) that all solutions converge to the largest invariant set in $\{(S(t), I(t)) \in \mathbb{R}^2_+ : V(S(t), I(t)) = 0\} = \{(S_*, I_*)\}$. This yields that the endemic equilibrium (S_*, I_*) is globally asymptotically stable in Ω_0. □

Lemma 2 *The level set* $\{(S, I) : V(S, I) < c\}$ *of the Lyapunov function* $V(S, I)$ *is convex for any* $c > 0$.

Proof Noting that the partial derivatives of $V(S, I)$ are V_S and V_I, thus

$$V_S = 1 - \frac{S_*}{S}\frac{1+\sigma S}{1+\sigma S_*},\ V_{SS} = \frac{S_*}{S^2(1+\sigma S_*)},\ V_I = 1 - \frac{I_*}{I},\ V_{II} = \frac{I_*}{I^2},\ V_{SI} = 0.$$

We obtain that the curvature ι of this level line $\{(S, I) :\ V(S, I) = c\}$ is

$$\iota = -\frac{V_{SS}V_I^2 + V_{II}V_S^2 - 2V_S V_I V_{SI}}{(V_S^2 + V_I^2)^{3/2}} = -\frac{V_{SS}V_I^2 + V_{II}V_S^2}{(V_S^2 + V_I^2)^{3/2}} < 0,$$

which confirms the convexity and completes the proof. □

C.2 Increment of Lyapunov function between adjacent switching events

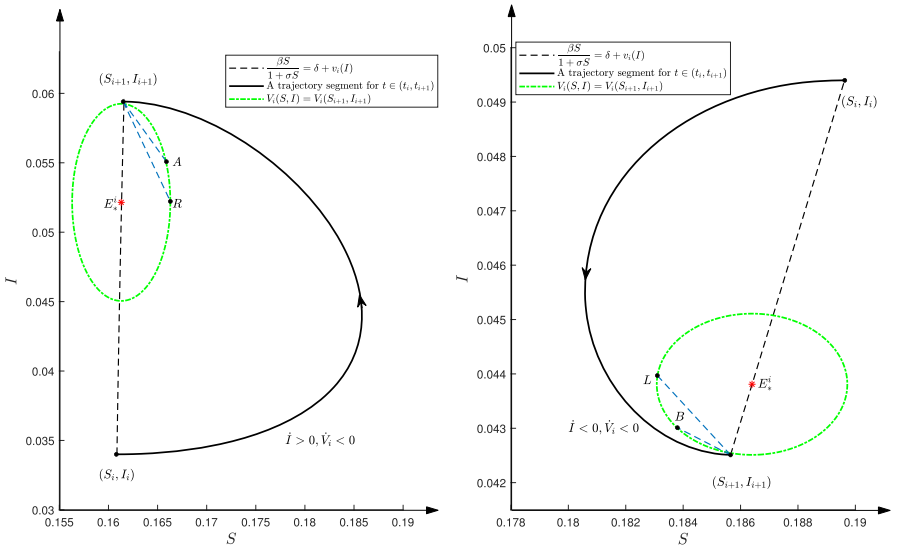
We now analyze the trajectory $(S(\cdot), I(\cdot), w(\cdot)) : \mathbb{R}_+ \to \Pi$ of model (2) with (16) and its projection $(S(\cdot), I(\cdot)) : \mathbb{R}_+ \to \Omega$. Let the set $\mathbb{T} = \{t_i\}$ consist of switching moments, where $0 = t_0 < t_1 < t_2 < \cdots$. We make the following observations:

(i) The trajectory segment $(S(t), I(t))$ on each time interval (t_i, t_{i+1}) is a solution of model (22) with $v(I) = v_{w(t_i)}(I)$, satisfying

$$\frac{\beta S(t)}{1+\sigma S(t)} \ne \delta + v(I(t)) \text{ for } t \in (t_i, t_{i+1}) \text{ and } \frac{\beta S(t_{i+1})}{1+\sigma S(t_{i+1})} = \delta + v(I(t_{i+1})). \tag{37}$$

(ii) If $\mathbb{T} = \{t_0, t_1, \cdots, t_n\}$ is finite, meaning that system (2) with (16) undergoes only a finite number of switching events, then trajectory segment $(S(t), I(t))$ on the time interval $(t_n, +\infty)$ is a solution of model (22) with $v(I) = v_{w(t_n)}(I)$, satisfying

$$\frac{\beta S(t)}{1+\sigma S(t)} \ne \delta + v_{w(t_n)}(I(t)) \text{ for } t \in (t_n, +\infty).$$



(a) $\frac{\beta S}{1+\sigma S} > \delta + v_i(I)$ (b) $\frac{\beta S}{1+\sigma S} < \delta + v_i(I)$

Fig. 14 A segment of an orbit of system (2) with (16) for (a) $I' > 0$, $V_i' < 0$; (b) $I' < 0$, $V_i' < 0$

From (ii) and Lemma 1, it follows that the trajectory of system (2) with (16) converges to an endemic equilibrium (node) when the sequence $\mathbb{T}$ is finite. This establishes conclusion (i) of Theorem 3.

Next, we analyze the case where an infinite number of switching events occur along a trajectory ((ii) in Theorem 3); i.e., when the set $\mathbb{T} = \{t_i\}$ is infinite. Denote

$$S_i = S(t_i), \quad I_i = I(t_i), \quad v_i(I) = v_{w(t_i)}(I)$$

Assuming that $V_i(S, I)$ is the Lyapunov function (35) for model (22) with $v(I) = v_{w(t_i)}(I)$, and (S_*^i, I_*^i) is its endemic equilibrium. The following lemma provides an estimate for the increment of the Lyapunov function $V_i(S, I)$ between adjacent switching events. Let

$$\Delta \bar{V}_i = V_i(S_{i+1}, I_{i+1}) - V_i(S_i, I_i). \tag{38}$$

Lemma 3 *If $\beta S(t)/(1+\sigma S(t)) > \delta + v_i(I(t))$ for $t \in (t_i, t_{i+1})$, then the increment of the Lyapunov function $V_i(S, I)$ between adjacent switching events t_i and t_{i+1} satisfies*

$$\Delta \bar{V}_i \le -\frac{1}{4}\mu(\delta + v_1)(I_{i+1} - I_*^i)\sqrt{S_r \int_{I_*^i}^{I_{i+1}} \left(1 - \frac{I_*^i}{\theta}\right) d\theta}, \tag{39}$$

where $R = (S_r, I_r)$ is the rightmost point of the level line $V_i(S, I) = V_i(S_{i+1}, I_{i+1})$ (see Fig. 14(a)).

Proof At the point $R = (S_r, I_r)$, we have

$$\frac{\partial V_i}{\partial I}(S_r, I_r) = 1 - \frac{I_*^i}{I_r} = 0,$$

that is $I_r = I_*^i$. Therefore $R = (S_r, I_*^i)$ and

$$V_i(S_r, I_*^i) = \int_{S_*^i}^{S_r} \left(1 - \frac{1+\sigma\theta}{1+\sigma S_*^i}\frac{S_*^i}{\theta}\right) d\theta.$$

We select a point $A = (S_a, I_a)$ on the arc of the level line $V_i(S, I) = V_i(S_{i+1}, I_{i+1})$ that connects (S_{i+1}, I_{i+1}) and R. By Lemma 2, it follows from that

$$\frac{I_*^i - I_{i+1}}{S_r - S_{i+1}} \le \frac{I_a - I_{i+1}}{S_a - S_{i+1}},$$

which yields

$$I_{i+1} - I_a \le \frac{S_a - S_{i+1}}{S_r - S_{i+1}}(I_{i+1} - I_*^i).$$

Further, we obtain

$$I_a - I_*^i \ge I_{i+1} - \frac{S_a - S_{i+1}}{S_r - S_{i+1}}(I_{i+1} - I_*^i) - I_*^i = \frac{S_r - S_a}{S_r - S_{i+1}}(I_{i+1} - I_*^i) \tag{40}$$

In the region

$$\left\{(S, I) \in \Omega \mid S > \frac{\delta + v_i(I)}{\beta - \sigma(\delta + v_i(I))}, I \ge I_*^i\right\},$$

we obtain

$$S_*^i = \frac{\delta + v_i(I_*^i)}{\beta - \sigma(\delta + v_i(I_*^i))} \le \frac{\delta + v_i(I)}{\beta - \sigma(\delta + v_i(I))}.$$

This means that

$$S - S_*^i \ge S - \frac{\delta + v_i(I)}{\beta - \sigma(\delta + v_i(I))} > 0.$$

It follows from the relation (36) that along the trajectory,

$$\begin{aligned}\frac{dV_i}{dI} = \frac{V_i'}{I'} &\le -\frac{\mu(S - S_*^i)^2(1+\sigma S)(\beta - \sigma(\delta + v_i(I)))}{SI(1+\sigma S_*^i)\left(S - \frac{\delta + v_i(I)}{\beta - \sigma(\delta + v_i(I))}\right)} \\ &\le -\frac{\mu(\delta + v_i(I))(S - S_*^i)}{SI} \le -\frac{\mu(\delta + v_1)(S - S_*^i)}{I}.\end{aligned}$$

Since V_i decreases along the solution, the restriction of the solution to the time interval (t_i, t_{i+1}) lies to the right of the level line $V_i(S, I) = V_i(S_{i+1}, I_{i+1})$ (as shown in

Fig. 14(a)). This means that for this restriction, $I_*^i \le I \le I_a$ leads to $S \ge S_a$ and

$$\frac{dV_i}{dI} \le -\frac{\mu(\delta+v_1)(S_a - S_*^i)}{I}. \tag{41}$$

Noting that $I'(t) > 0$ for $t \in (t_i, t_{i+1})$, we conclude that the restriction of the trajectory to this time interval is parameterized as $(\hat{S}(I), I)$ for $I \in [I_i, I_{i+1}]$. Accordingly, we integrate (41) over the interval $[I_*^i, I_a] \subset [I_i, I_{i+1}]$ to obtain

$$V_i(\hat{S}(I_a), I_a) - V_i(\hat{S}(I_*^i), I_*^i) \le -\mu(\delta+v_1)(S_a - S_*^i)\ln\frac{I_a}{I_*^i}.$$

Using the inequality $\ln(1+x) \ge x/(1+x)$ for $x \ge -1$, we obtain

$$\begin{aligned} V_i(\hat{S}(I_a), I_a) - V_i(\hat{S}(I_*^i), I_*^i) &\le -\mu(\delta+v_1)(S_a - S_*^i)\frac{(I_a - I_*^i)}{I_a} \\ &\le -\mu(\delta+v_1)(S_a - S_*^i)(I_a - I_*^i). \end{aligned}$$

Furthermore, since (40),

$$V_i(\hat{S}(I_a), I_a) - V_i(\hat{S}(I_*^i), I_*^i) \le -\frac{\mu(\delta+v_1)(S_a - S_*^i)(S_r - S_a)(I_{i+1} - I_*^i)}{S_r - S_{i+1}}. \tag{42}$$

The maximum value of the function $h(S_a) := \frac{(S_a - S_*^i)(S_r - S_a)}{S_r - S_{i+1}}$ for $S_a \in [S_{i+1}, S_r] \subset [S_*^i, S_r]$ is obtained at $S_a = \frac{S_*^i + S_r}{2}$; i.e.,

$$\max_{S_a \in [S_{i+1}, S_r]} h(S_a) = \frac{(S_r - S_*^i)^2}{4(S_r - S_{i+1})} \ge \frac{S_r - S_*^i}{4}.$$

Hence, it follows from (42) that

$$V_i(\hat{S}(I_a), I_a) - V_i(\hat{S}(I_*^i), I_*^i) \le -\frac{\mu(\delta+v_1)(S_r - S_*^i)(I_{i+1} - I_*^i)}{4}.$$

From the fact that V_i is decreasing along the trajectory, this estimate suggests that

$$\Delta\bar{V}_i \le V_i(\hat{S}(I_a), I_a) - V_i(\hat{S}(I_*^i), I_*^i) \le -\frac{\mu(\delta+v_1)(S_r - S_*^i)(I_{i+1} - I_*^i)}{4}. \tag{43}$$

In the following, we estimate $S_r - S_*^i$. Since $V_i(S_r, I_*^i) = V_i(S_{i+1}, I_{i+1})$, this implies that

$$\int_{S_*^i}^{S_r}\left(1 - \frac{1+\sigma\theta}{1+\sigma S_*^i}\frac{S_*^i}{\theta}\right)d\theta = \int_{S_*^i}^{S_{i+1}}\left(1 - \frac{1+\sigma\theta}{1+\sigma S_*^i}\frac{S_*^i}{\theta}\right)d\theta + \int_{I_*^i}^{I_{i+1}}\left(1 - \frac{I_*^i}{\theta}\right)d\theta,$$

which yields

$$\int_{S_{i+1}}^{S_r}\left(1-\frac{1+\sigma\theta}{1+\sigma S_*^i}\frac{S_*^i}{\theta}\right)d\theta=\int_{I_*^i}^{I_{i+1}}\left(1-\frac{I_*^i}{\theta}\right)d\theta. \tag{44}$$

Further, we estimate the left-hand side of (44),

$$\begin{aligned}\int_{S_{i+1}}^{S_r}\left(1-\frac{1+\sigma\theta}{1+\sigma S_*^i}\frac{S_*^i}{\theta}\right)d\theta &= S_r-S_{i+1}-\frac{S_*^i}{1+\sigma S_*^i}\left(\ln\frac{S_r}{S_{i+1}}+\sigma(S_r-S_{i+1})\right)\\ &\le S_r-S_{i+1}-\frac{1+\sigma S_r}{1+\sigma S_r^i}\frac{S_*^i(S_r-S_{i+1})}{S_r}\\ &\le S_r-S_{i+1}-\frac{S_*^i(S_r-S_{i+1})}{S_r}.\end{aligned}$$

Hence,

$$\int_{I_*^i}^{I_{i+1}}\left(1-\frac{I_*^i}{\theta}\right)d\theta\le\frac{(S_r-S_*^i)(S_r-S_{i+1})}{S_r}.$$

Due to $S_*^i<S_{i+1}$, we conclude that

$$(S_r-S_*^i)^2\ge S_r\int_{I_*^i}^{I_{i+1}}\left(1-\frac{I_*^i}{\theta}\right)d\theta.$$

Combining with (43), we get

$$\Delta\bar{V}_i\le-\frac{1}{4}\mu(\delta+v_1)(I_{i+1}-I_*^i)\sqrt{S_r\int_{I_*^i}^{I_{i+1}}\left(1-\frac{I_*^i}{\theta}\right)d\theta}.$$

□

C.3 Change in Lyapunov functions at a switching point

In this subsection, we estimate the increment between the Lyapunov functions $V_i(S,I)$ and $V_{i+1}(S,I)$ at the switching point (S_{i+1},I_{i+1}). Let

$$\Delta\hat{V}_i=V_{i+1}(S_{i+1},I_{i+1})-V_i(S_{i+1},I_{i+1}). \tag{45}$$

Lemma 4 *If $\beta S(t)/(1+\sigma S(t))>\delta+v_i(I(t))$ for $t\in(t_i,t_{i+1})$, then*

$$0\le I_*^i-I_*^{i+1}\le l\mu C(I_{i+1}-I_*^i), \tag{46}$$

where

$$C=\frac{1}{(\delta+v_i(I_*^i))(\delta+v_{i+1}(I_*^{i+1}))}+\frac{\sigma}{(\beta-\sigma(\delta+v_i(I_*^i)))(\beta-\sigma(\delta+v_{i+1}(I_*^{i+1})))}>0. \tag{47}$$

Proof For the branch $v_i(I)$ of the Preisach operator, the endemic equilibrium (S_*^i, I_*^i) of system (22) with $v(I) = v_i(I)$ satisfies

$$S_*^i = \frac{\delta + v_i(I_*^i)}{\beta - \sigma(\delta + v_i(I_*^i))}, \quad I_*^i = \mu\left(\frac{1}{\delta + v_i(I_*^i)} - \frac{S_*^i}{\delta + v_i(I_*^i)}\right).$$

Thus,

$$\begin{aligned} I_*^i - I_*^{i+1} &= \mu\left(\frac{1}{\delta + v_i(I_*^i)} - \frac{S_*^i}{\delta + v_i(I_*^i)} - \frac{1}{\delta + v_{i+1}(I_*^{i+1})} + \frac{S_*^{i+1}}{\delta + v_{i+1}(I_*^{i+1})}\right) \\ &= \mu\Bigg(\frac{1}{\delta + v_i(I_*^i)} - \frac{1}{\delta + v_{i+1}(I_*^{i+1})} + \frac{1}{\beta - \sigma(\delta + v_{i+1}(I_*^{i+1}))} \\ &\quad - \frac{1}{\beta - \sigma(\delta + v_i(I_*^i))}\Bigg) \\ &= \mu C(v_{i+1}(I_*^{i+1}) - v_{i+1}(I_*^i) + v_{i+1}(I_*^i) - v_i(I_*^i)) \\ &= \mu C(v'_{i+1}(\hat{I})(I_*^{i+1} - I_*^i) + v_{i+1}(I_*^i) - v_i(I_*^i)) \end{aligned}$$

where $\hat{I}$ lies between I_*^i and I_*^{i+1}, and C is defined by (47).

Now, assuming $I_*^{i+1} > I_*^i$, we obtain

$$0 > I_*^i - I_*^{i+1} = \mu C(v'_{i+1}(\hat{I})(I_*^{i+1} - I_*^i) + v_{i+1}(I_*^i) - v_i(I_*^i)) \geq 0,$$

since $v_{i+1}(I)$ increasing. Moreover, (21) implies

$$0 \leq v_{i+1}(I_*^i) - v_i(I_*^i) \leq l(I_{i+1} - I_*^i). \tag{48}$$

This leads to a contradiction, meaning that $I_*^{i+1} \leq I_*^i$. Consequently, $S_*^{i+1} \geq S_*^i$ and

$$I_*^i - I_*^{i+1} \leq \mu C(v_{i+1}(I_*^i) - v_i(I_*^i)) \leq l\mu C(I_{i+1} - I_*^i).$$

□

Lemma 5 *If $\beta S(t)/(1 + \sigma S(t)) > \delta + v_i(I(t))$ for $t \in (t_i, t_{i+1})$, then the increment between Lyapunov functions at the switching point (S_{i+1}, I_{i+1}) satisfies*

$$\Delta \hat{V}_i \leq l\mu C(l\mu C + 1)\frac{(I_{i+1} - I_*^i)^2}{I_*^i}, \tag{49}$$

where C is defined by (47).

Proof Based on the form of the Lyapunov function (35), we express $\Delta \hat{V}_i$ defined in (45) as $\Delta \hat{V}_i = \Delta_S + \Delta_I$, where

$$\begin{aligned}\Delta_S &= \int_{S_*^{i+1}}^{S_{i+1}} \left(1 - \frac{1+\sigma\theta}{1+\sigma S_*^{i+1}} \frac{S_*^{i+1}}{\theta}\right) d\theta - \int_{S_*^i}^{S_{i+1}} \left(1 - \frac{1+\sigma\theta}{1+\sigma S_*^i} \frac{S_*^i}{\theta}\right) d\theta \\ &= -\int_{S_*^i}^{S_*^{i+1}} \left(1 - \frac{1+\sigma\theta}{1+\sigma S_*^i} \frac{S_*^i}{\theta}\right) d\theta - \int_{S_*^{i+1}}^{S_{i+1}} \frac{1+\sigma\theta}{\theta} \left(\frac{S_*^{i+1}}{1+\sigma S_*^{i+1}} - \frac{S_*^i}{1+\sigma S_*^i}\right) d\theta,\end{aligned}$$

and

$$\begin{aligned}\Delta_I &= \int_{I_*^{i+1}}^{I_{i+1}} \left(1 - \frac{I_*^{i+1}}{\theta}\right) d\theta - \int_{I_*^i}^{I_{i+1}} \left(1 - \frac{I_*^i}{\theta}\right) d\theta \\ &= -\int_{I_*^i}^{I_{i+1}} \left(\frac{I_*^{i+1} - I_*^i}{\theta}\right) d\theta - \int_{I_*^i}^{I_*^{i+1}} \left(1 - \frac{I_*^{i+1}}{\theta}\right) d\theta.\end{aligned}$$

Since $S_*^i \le S_*^{i+1} \le S_{i+1}$ (by Lemma 4), we obtain

$$\int_{S_*^i}^{S_*^{i+1}} \left(1 - \frac{1+\sigma\theta}{1+\sigma S_*^i} \frac{S_*^i}{\theta}\right) d\theta \ge 0, \quad \int_{S_*^{i+1}}^{S_{i+1}} \frac{1+\sigma\theta}{\theta} \left(\frac{S_*^{i+1}}{1+\sigma S_*^{i+1}} - \frac{S_*^i}{1+\sigma S_*^i}\right) d\theta \ge 0,$$

which implies that $\Delta_S \le 0$. Thus,

$$\Delta \hat{V}_i \le \Delta_I = -\int_{I_*^i}^{I_{i+1}} \left(\frac{I_*^{i+1} - I_*^i}{\theta}\right) d\theta - \int_{I_*^i}^{I_*^{i+1}} \left(1 - \frac{I_*^{i+1}}{\theta}\right) d\theta. \tag{50}$$

Next, we estimate the first integral in (50). Since $I_*^{i+1} \le I_*^i \le I_{i+1}$ (by Lemma 4), it follows that

$$0 \le -\int_{I_*^i}^{I_{i+1}} \left(\frac{I_*^{i+1} - I_*^i}{\theta}\right) d\theta \le \frac{(I_*^i - I_*^{i+1})(I_{i+1} - I_*^i)}{I_*^i} \le l\mu C \frac{(I_{i+1} - I_*^i)^2}{I_*^i}, \tag{51}$$

where C is defined by (47). On the other hand,

$$0 \le -\int_{I_*^i}^{I_*^{i+1}} \left(1 - \frac{I_*^{i+1}}{\theta}\right) d\theta \le \frac{(I_*^i - I_*^{i+1})^2}{I_*^i} \le l^2\mu^2 C^2 \frac{(I_{i+1} - I_*^i)^2}{I_*^i}. \tag{52}$$

Combining (50), (51), and (52), we obtain (49). □

C.4 Estimate of $V_{i+1}(S_{i+1}, I_{i+1}) - V_i(S_i, I_i)$

By combining Lemmas 3 and 5, we derive an estimate for the increment over an entire switching event. Let

$$\Delta V_i = V_{i+1}(S_{i+1}, I_{i+1}) - V_i(S_i, I_i). \tag{53}$$

Lemma 6 *If $\beta S(t)/(1+\sigma S(t)) > \delta + v_i(I(t))$ for $t \in (t_i, t_{i+1})$, then the increment ΔV_i satisfies*

$$\Delta V_i \le -M_i (I_{i+1} - I_*^i)^2, \tag{54}$$

with

$$M_i = \frac{\mu(\delta+v_1)}{4}\sqrt{\frac{S_r}{2I_{i+1}}} - \frac{l\mu C(l\mu C+1)}{I_*^i}, \tag{55}$$

where $R = (S_r, I_r)$ is the rightmost point of the level line $V_i(S, I) = V_i(S_{i+1}, I_{i+1})$, and C is defined by (47).

Proof Using the inequality $2(1+x)\ln(1+x) \le x(2+x)$ for $x \ge 0$, we obtain

$$\begin{aligned}\int_{I_*^i}^{I_{i+1}} \left(1 - \frac{I_*^i}{\theta}\right) d\theta &= I_{i+1} - I_*^i - I_*^i \ln \frac{I_{i+1}}{I_*^i} \\ &\ge I_{i+1} - I_*^i - I_*^i \frac{I_{i+1}^2 - (I_*^i)^2}{2I_{i+1}I_*^i} \\ &= \frac{(I_{i+1} - I_*^i)^2}{2I_{i+1}}.\end{aligned} \tag{56}$$

Substituting this estimate into (39) and combining it with (49), we derive (54). □

Lemma 7 *If $\beta S(t)/(1+\sigma S(t)) < \delta + v_i(I(t))$ for $t \in (t_i, t_{i+1})$, then the increment ΔV_i satisfies*

$$\Delta V_i \le -N_i (I_{i+1} - I_*^i)^2, \tag{57}$$

with

$$N_i = \frac{\mu(\delta+v_1)}{4}\sqrt{\frac{S_l}{2I_{i+1}}} - l\mu C\left(\frac{l\mu C}{I_*^i} + \frac{1}{I_{i+1}}\right), \tag{58}$$

where $L = (S_l, I_l)$ is the leftmost point of the level line $V_i(S, I) = V_i(S_{i+1}, I_{i+1})$ (see Fig. 14(b)).

Proof We apply the methods from Lemms 3-6 to derive an estimate for ΔV_i when $\beta S(t)/(1+\sigma S(t)) < \delta + v_i(I(t))$ for $t \in (t_i, t_{i+1})$, implying $I' < 0$. For completeness, we provide an overview of the main proof process.

The value of $V_i(S, I)$ at the point $L = (S_l, I_l) = (S_l, I_*^i)$ satisfies

$$V_i(S_l, I_*^i) = \int_{S_*^i}^{S_l} \left(1 - \frac{1+\sigma\theta}{1+\sigma S_*^i}\frac{S_*^i}{\theta}\right) d\theta = V_i(S_{i+1}, I_{i+1}).$$

We select a point $B = (S_b, I_b)$ on the arc of the level line $V_i(S, I) = V_i(S_{i+1}, I_{i+1})$, which connects (S_{i+1}, I_{i+1}) and L. By Lemma 2, it follows that

$$I_*^i - I_b \ge I_*^i - I_{i+1} - \frac{S_{i+1} - S_b}{S_{i+1} - S_l}(I_*^i - I_{i+1}) = \frac{S_b - S_l}{S_{i+1} - S_l}(I_*^i - I_{i+1}) \tag{59}$$

In the domain

$$\left\{(S, I) \in \Omega_0 \mid S < \frac{\delta + v_i(I)}{\beta - \sigma(\delta + v_i(I))}, I \le I_*^i\right\},$$

we obtain

$$S_*^i = \frac{\delta + v_i(I_*^i)}{\beta - \sigma(\delta + v_i(I))} \ge \frac{\delta + v_i(I)}{\beta - \sigma(\delta + v_i(I))}.$$

This implies

$$0 < \frac{\delta + v_i(I)}{\beta - \sigma(\delta + v_i(I))} - S \le S_*^i - S.$$

It follows from (36) that along the trajectory,

$$\begin{aligned}\frac{dV_i}{dI} &\ge \frac{\mu(S - S_*^i)^2(1 + \sigma S)(\beta - \sigma(\delta + v_i(I)))}{SI(1 + \sigma S_*^i)\left(\frac{\delta + v_i(I)}{\beta - \sigma(\delta + v_i(I))} - S\right)} \\ &\ge \frac{\mu(\delta + v_i(I))(S_*^i - S)}{SI} \ge \frac{\mu(\delta + v_1)(S_*^i - S)}{I}.\end{aligned}$$

Since the trajectory segment on $[I_b, I_*^i]$ lies to the left of the level line $V_i(S, I) = V_i(S_{i+1}, I_{i+1})$, we have $S \le S_b$ and

$$\frac{dV_i}{dI} \ge \frac{\mu(\delta + v_1)(S_*^i - S_b)}{I}$$

This implies that

$$V_i(\hat{S}(I_*^i), I_*^i) - V_i(\hat{S}(I_b), I_b) \ge \mu(\delta + v_1)(S_*^i - S_b) \ln \frac{I_*^i}{I_b},$$

where $(\hat{S}(I), I)$ is a parameterization of the trajectory segment with $I \in [I_{i+1}, I_i]$. Using the inequality $\ln(1 + x) \ge x/(1 + x)$ for $x \ge -1$ and (59), with $I_*^i \le 1$, we obtain

$$\begin{aligned}V_i(\hat{S}(I_b), I_b) - V_i(\hat{S}(I_*^i), I_*^i) &\le -\mu(\delta + v_1)(S_*^i - S_b)\frac{I_*^i - I_b}{I_*^i} \\ &\le -\frac{\mu(\delta + v_1)(S_*^i - S_b)(S_b - S_l)(I_*^i - I_{i+1})}{(S_{i+1} - S_l)}.\end{aligned}$$

Following the steps in Lemma 3, maximizing the right-hand side of this inequality over $S_b \in [S_l, S_{i+1}]$ and noting that V_i decreases along the trajectory, we derive

$$\Delta \bar{V}_i \le V_i(\hat{S}(I_b), I_b) - V_i(\hat{S}(I_*^i), I_*^i) \le -\frac{\mu(\delta + v_1)(S_*^i - S_l)(I_*^i - I_{i+1})}{4}. \quad (60)$$

Next, we estimate $S_*^i - S_l$ in (60). Since the Lyapunov function V_i has the same value at points (S_l, I_*^i) and (S_{i+1}, I_{i+1}), we obtain

$$\int_{S_l}^{S_{i+1}} \left(\frac{1+\sigma\theta}{1+\sigma S_*^i} \frac{S_*^i}{\theta} - 1 \right) d\theta = \int_{I_{i+1}}^{I_*^i} \left(\frac{I_*^i}{\theta} - 1 \right) d\theta.$$

Furthermore,

$$\int_{S_l}^{S_{i+1}} \left(\frac{1+\sigma\theta}{1+\sigma S_*^i} \frac{S_*^i}{\theta} - 1 \right) d\theta \leq S_l - S_{i+1} - \frac{S_*^i(S_l - S_{i+1})}{S_l} \leq \frac{(S_*^i - S_l)^2}{S_l},$$

where $S_l < S_{i+1} < S_*^i$. Hence,

$$\frac{(S_*^i - S_l)^2}{S_l} \geq \int_{I_{i+1}}^{I_*^i} \left(\frac{I_*^i}{s} - 1 \right) ds.$$

From (60), we conclude

$$\Delta \bar{V}_i \leq -\frac{1}{4}\mu(\delta + v_1)(I_*^i - I_{i+1}) \sqrt{S_l \int_{I_{i+1}}^{I_*^i} \left(\frac{I_*^i}{\theta} - 1 \right) d\theta}.$$

Since (56), we obtain

$$\Delta \bar{V}_i \leq -\frac{1}{4}\mu(\delta + v_1)(I_*^i - I_{i+1})^2 \sqrt{\frac{S_l}{2I_{i+1}}}. \tag{61}$$

Following the proof of Lemma 4,

$$I_*^{i+1} - I_*^i = \mu C[v'_{i+1}(\hat{I})(I_*^i - I_*^{i+1}) + v_i(I_*^i) - v_{i+1}(I_*^i)],$$

where

$$0 \leq v_i(I_*^i) - v_{i+1}(I_*^i) \leq l(I_*^i - I_{i+1}). \tag{62}$$

Thus, we conclude that $I_*^{i+1} \geq I_*^i$ and $S_*^{i+1} \leq S_*^i$, given that $v'_{i+1}(\hat{I}) \geq 0$. Furthermore, we establish the estimate

$$0 \leq I_*^{i+1} - I_*^i \leq l\mu C(I_*^i - I_{i+1}). \tag{63}$$

Contrary to the case considered in Lemmas 3-5, we obtain

$$S_{i+1} \leq S_*^{i+1} \leq S_*^i, \quad I_{i+1} \leq I_*^i \leq I_*^{i+1}. \tag{64}$$

Similarly, using the notations Δ_S and Δ_I from Lemma 5, we deduce from (64) that $\Delta_S \le 0$. Consequently, the difference in (45) satisfies (50), and (51) is rewritten as

$$0 \le -\int_{I_*^i}^{I_{i+1}} \left(\frac{I_*^{i+1} - I_*^i}{\theta}\right) d\theta \le \frac{(I_*^{i+1} - I_*^i)(I_*^i - I_{i+1})}{I_{i+1}} \le l\mu C \frac{(I_{i+1} - I_*^i)^2}{I_{i+1}}, \tag{65}$$

Combining (50), (52) and (65), we obtain

$$\Delta \hat{V}_i \le l\mu C \left(\frac{l\mu C}{I_*^i} + \frac{1}{I_{i+1}}\right)(I_{i+1} - I_*^i)^2.$$

Adding this estimate to (61) gives

$$\Delta V_i \le -\mu \left(\frac{\delta + v_1}{4}\sqrt{\frac{S_l}{2I_{i+1}}} - lC\left(\frac{l\mu C}{I_*^i} + \frac{1}{I_{i+1}}\right)\right)(I_{i+1} - I_*^i)^2.$$

□

Lemma 8 *For $t \ge t_2$, we have*

$$\begin{aligned} S(t) &\ge \bar{S} := \frac{\delta + v_1}{\beta - \sigma(\delta + v_1)} \exp\left(-\left(1 + \frac{2(\beta - \sigma(\delta + v_1))}{\delta + v_1}\right)\left(\sigma + \frac{\beta - \sigma(\delta + v_1)}{\delta + v_1}\right)\right), \\ I(t) &\ge \bar{I} := \frac{\mu(\beta - \delta - v_2)}{\beta(\delta + v_2)} \exp\left(1 + \frac{2\beta(\delta + v_2)}{\mu(\beta - \delta - v_2)}\right). \end{aligned} \tag{66}$$

Proof At the point

$$(S_i, I_i) = \left(\frac{\delta + v_i(I_i)}{\beta - \sigma(\delta + v_i(I_i))}, I_i\right),$$

where the solution satisfies $S' < 0$ and $I' = 0$ (see Fig. 14(b)), we have

$$V_i(S_i, I_i) = \int_{S_*^i}^{S_i} \left(1 - \frac{1 + \sigma\theta}{1 + \sigma S_*^i}\frac{S_*^i}{\theta}\right) d\theta + \int_{I_*^i}^{I_i} \left(1 - \frac{I_*^i}{\theta}\right) d\theta \le S_i - S_*^i + I_i - I_*^i \le 2.$$

Notice that the minimum $\bar{s}_m^i = \min_{t\in[t_i, t_{i+2}]} S(t)$ of the $S-$value of the solution on the interval $[t_i, t_{i+2}]$ occurs at $t_m^i \in [t_i, t_{i+1}]$, i.e., $\bar{s}_m^i = S(t_m^i)$. Since $V_i(S_i, I_i) \le 2$ and V_i decreases for $t \in [t_i, t_{i+1}]$, it follows that

$$2 \ge V_i(S(t_m^i), I(t_m^i)) \ge \int_{\bar{s}_m^i}^{S_*^i} \left(\frac{1 + \sigma\theta}{1 + \sigma S_*^i}\frac{S_*^i}{\theta} - 1\right) d\theta \ge \frac{S_*^i}{1 + \sigma S_*^i} \ln \frac{S_*^i}{\bar{s}_m^i} - S_*^i.$$

Hence, $\bar{s}_m^i \geq S_*^i \exp\left(-(1+\frac{2}{S_*^i})(\sigma+\frac{1}{S_*^i})\right)$, and since $S_*^i \geq (\delta+v_1)/(\beta-\sigma(\delta+v_1))$, we obtain

$$\bar{s}_m^i = \min_{t\in[t_i,t_{i+2}]} S(t) \geq \frac{\delta+v_1}{\beta-\sigma(\delta+v_1)} \exp\left(-\left(1+\frac{2(\beta-\sigma(\delta+v_1))}{\delta+v_1}\right) \times \left(\sigma+\frac{\beta-\sigma(\delta+v_1)}{\delta+v_1}\right)\right).$$

On the other hand, the minimum $\bar{i}_m^i = \min_{t\in[t_i,t_{i+2}]} I(t)$ of the $I-$value of the solution on the interval $[t_i, t_{i+2}]$ is attained at (S_{i+1}, I_{i+1}), i.e., $\bar{i}_m^i = I_{i+1}$. Similarly, we have

$$2 \geq V_i(S_{i+1}, I_{i+1}) \geq \int_{I_{i+1}}^{I_*^i} \left(\frac{I_*^i}{\theta}-1\right) d\theta \geq I_*^i \ln\frac{I_*^i}{I_{i+1}} - I_*^i,$$

and

$$I_{i+1} \geq I_*^i \exp(-(1+\frac{2}{I_*^i})).$$

Since

$$I_*^i = \frac{\mu}{\delta+v_i(I_*^i)}\left(1-S_*^i\right) \quad \text{and} \quad S_*^i \leq \frac{\delta+v_2}{\beta-\sigma(\delta+v_2)},$$

it follows that

$$I_{i+1} = \min_{t\in[t_i,t_{i+2}]} I(t) \geq \frac{\mu(\beta-\delta-v_2)}{\beta(\delta+v_2)} \exp\left(1+\frac{2\beta(\delta+v_2)}{\mu(\beta-\delta-v_2)}\right),$$

which completes the proof. □

Next, we demonstrate that all trajectories of system (2) with (16) converge to the continuum set of endemic equilibria.

Lemma 9 *All trajectories of system* (2) *with* (16) *converge to the continuum set of endemic equilibria* E_κ^*, *where* $\kappa^* \in [0,1]$. *Here* $\epsilon \in (0, \mathcal{R}_{01}-1)$ *is chosen such that* $d > 0$ *defined in* (68).

Proof Based on Lemmas 6-8, we conclude that the sequence $V_i(S_i, I_i)$ satisfies

$$\Delta V_i = V_{i+1}(S_{i+1}, I_{i+1}) - V_i(S_i, I_i) \leq -d(I_*^i - I_{i+1})^2, \quad i = 0, 1, 2, \cdots, \tag{67}$$

with

$$d := \frac{\mu(\delta+v_1)}{4}\sqrt{\frac{\bar{S}}{2}} - \frac{l\mu C_0(l\mu C_0+1)}{\bar{I}}, \tag{68}$$

which is independent of i, and

$$C_0 := \frac{1}{(\delta+v_1)^2} + \frac{\sigma}{(\beta-\sigma(\delta+v_2))^2}. \tag{69}$$

Since $0 \le S \le 1$ and $0 \le I \le 1$, it follows that

$$\begin{aligned} \frac{(S-S_*^i)^2}{2\bar{S}} &\ge \int_{S_*^i}^{S} \left(1 - \frac{1+\sigma\theta}{1+\sigma S_*^i}\frac{S_*^i}{\theta}\right) d\theta \ge \frac{(S-S_*^i)^2}{2}, \\ \frac{(I-I_*^i)^2}{2\bar{I}} &\ge \int_{I_*^i}^{I} \left(1 - \frac{I_*^i}{\theta}\right) d\theta \ge \frac{(I-I_*^i)^2}{2}, \end{aligned} \tag{70}$$

where $\bar{S}$ and $\bar{I}$ are defined in (66). Furthermore,

$$\frac{(S-S_*^i)^2}{2\bar{S}} + \frac{(I-I_*^i)^2}{2\bar{I}} \ge V_i(S,I) \ge \frac{(S-S_*^i)^2}{2} + \frac{(I-I_*^i)^2}{2}. \tag{71}$$

From (67), we obtain

$$V_n = V_1 + \sum_{i=1}^{n-1} \Delta V_i \le V_1 - d\sum_{i=1}^{n-1} (I_*^i - I_{i+1})^2,$$

and since the Lyapunov function satisfies $V_n \ge 0$ for any n, we have

$$\sum_{i=1}^{n-1} (I_*^i - I_{i+1})^2 \le \frac{V_1}{d}.$$

This leads to

$$\sum_{i=1}^{+\infty} (I_*^i - I_{i+1})^2 < +\infty;$$

i.e., $I_{i+1} - I_*^i \to 0$ when $i \to +\infty$. Due to (63), $I_i - I_*^i \to 0$.

$$S_i = \frac{(\delta + v_i(I_i))}{\beta - \sigma(\delta + v_i(I_i))}$$

and

$$S_i^* = \frac{(\delta + v_i(I_*^i))}{\beta - \sigma(\delta + v_i(I_*^i))}$$

mean that $S_i - S_*^i \to 0$. From (71), we conclude that $V_i(S_i, I_i) \to 0$ as $i \to +\infty$. Since $V_i \ge 0$ and V_i decreases along the trajectory, we obtain

$$V_i(S_i, I_i) = \max_{t\in[t_i, t_{i+1}]} V_i(S(t), I(t)) \to 0, \quad \text{as } i \to +\infty.$$

Thus, all trajectories converge to the continuum set of endemic equilibria due to (71). □

Finally, we demonstrate that every trajectory of system (2) with (16) converges to a point in the continuum of endemic equilibria E_κ^*, where $\kappa^* \in [0, 1]$.

Lemma 10 *Each trajectory of system* (2) *with* (16) *converges to an endemic equilibrium* E^*_κ *for some* $\kappa^* \in [0, 1]$.

Proof From (71), it follows that

$$V_i(S_{i+1}, I_{i+1}) \le \frac{(S_{i+1} - S^i_*)^2}{2\bar{S}} + \frac{(I_{i+1} - I^i_*)^2}{2\bar{I}}.$$

Observing that

$$\left|S_{i+1} - S^i_*\right| = \left|\frac{\delta + v_i(I_{i+1})}{\beta - \sigma(\delta + v_i(I_{i+1}))} - \frac{\delta + v_i(I^i_*)}{\beta - \sigma(\delta + v_i(I^i_*))}\right| \le \frac{l}{\beta - (\delta + v_2)}\left|I_{i+1} - I^i_*\right|,$$

we obtain

$$V_i(S_{i+1}, I_{i+1}) \le c_1(I_{i+1} - I^i_*)^2, \quad c_1 = \frac{l^2}{2(\beta - (\delta + v_2))^2\bar{S}} + \frac{1}{2\bar{I}}. \tag{72}$$

From Lemma 5, we have

$$\Delta\hat{V}_i \le c_2(I_{i+1} - I^i_*)^2, \quad c_2 = \frac{l\mu C_0(l\mu C_0 + 1)}{\bar{I}},$$

where C_0 is defined by (69). Using (72), we derive

$$V_{i+1}(S_{i+1}, I_{i+1}) = V_i(S_{i+1}, I_{i+1}) + \Delta\hat{V}_i \le (c_1 + c_2)(I_{i+1} - I^i_*)^2. \tag{73}$$

When $V_i(S_i, I_i) \ge (c_1 + c_2 + d)(I_{i+1} - I^i_*)^2$, where d is defined by (68), we obtain

$$V_{i+1}(S_{i+1}, I_{i+1}) \le \frac{c_1 + c_2}{c_1 + c_2 + d} V_i(S_i, I_i). \tag{74}$$

On the other hand, if $V_i(S_i, I_i) \le (c_1 + c_2 + d)(I_{i+1} - I^i_*)^2$, then (67) implies (74). Consequently, we have

$$V_i(S_i, I_i) \le V_0\left(\frac{c_1 + c_2}{c_1 + c_2 + d}\right)^i$$

in both cases. Since V_i decreases along the trajectory, we obtain $V_i(S_{i+1}, I_{i+1}) \le V_i(S_i, I_i)$. Moreover, from (71),

$$V_i(S_{i+1}, I_{i+1}) \ge \frac{(I_{i+1} - I^i_*)^2}{2},$$

which implies

$$\frac{(I_{i+1} - I^i_*)^2}{2} \le V_i(S_i, I_i) \le V_1\left(\frac{c_1 + c_2}{c_1 + c_2 + d}\right)^i.$$

Applying (46) and (63), we deduce

$$\left|I_*^{i+1} - I_*^i\right| \le l\mu C_0 \left|I_{i+1} - I_*^i\right|.$$

Thus,

$$\left|I_*^{i+1} - I_*^i\right| \le l\mu C_0\sqrt{2V_1}\left(\frac{c_1+c_2}{c_1+c_2+d}\right)^{\frac{i}{2}}.$$

This implies that I_*^i forms a Cauchy sequence and converges to some limit I_*. Since $I_{i+1} - I_*^i \to 0$ as $i \to +\infty$, we conclude that $I(t) \to I_*$ as $t \to +\infty$. Consequently, $S(t)$ also converges to some limit, denoted S_*. Thus this trajectory converges to the endemic equilibrium (S_*, I_*). □

Acknowledgements This work was supported by Major International (Regional) Joint Research Project of National Natural Science Foundation of China (12220101001, YX), and by National Natural Science Foundation of China (12031010, YX). HW was a recipient of Chinese Scholarship Council (CSC) funding.

Data Availability All data generated or analyzed during this study is included in this article.

Declarations

Conflicts of Interest The authors declare that they have no Conflict of interest.

References

Bernardo MD, Budd C, Champneys A, Kowalczyk P (2008) Piecewise-Smooth Dynamical Systems: Theory and Applications. Springer,

Brokate M, Sprekels J (1996) Hysteresis and Phase Transitions. Springer-Verlag

Di Bernardo MC, Crowther-Swanepoel D, Broderick P, Webb E, Sellick G, Wild R, Sullivan K, Vijayakrishnan J, Wang Y, Pittman AM, Sunter NJ, Hall AG, Dyer MJ, Matutes E, Dearden C, Mainoufowler T, Jackson GH, Summerfield G, Harris RJ, Pettitt AR, Hillmen P, Allsup DJ, Bailey JR, Pratt G, Pepper C, Fegan C, Allan JM, Catovsky D, Houlston RS (2008) A genome-wide association study identifies six susceptibility loci for chronic lymphocytic leukemia. Nat Genet 40:1204–1210

d'Onofrio A, Piero M (2009) Information-related changes in contact patterns may trigger oscillations in the endemic prevalence of infectious diseases. J Theor Biol 256:473–478

Erdem M, Safan M, Castillo-Chavez C (2017) Mathematical analysis of an SIQR influenza model with imperfect quarantine. Bull Math Biol 79:1612–1636

Fairlie R (2020) The impact of COVID-19 on small business owners: Evidence from the first three months after widespread social-distancing restrictions. J Econ Manag Strategy 29:727–740

Feng Z, Thieme H (1995) Recurrent outbreaks of childhood diseases revisited: The impact of isolation. Math Biosci 128:93–130

Guan R, Kopfová J, Rachinskii D (2024) Global stability of SIR model with heterogeneous transmission rate modeled by the Preisach operator. SIAM J Appl Dyn Syst 23:1199–1241

Gurevich P, Rachinskii D (2015) Pattern formation in parabolic equations containing hysteresis with diffusive thresholds. J Math Anal Appl 424:1103–1124

Hale JK, Lunel SMV (1993) Introduction to Functional Differential Equations. Springer

Herbert H, Ma Z, Liao S (2002) Effects of quarantine in six endemic models for infectious diseases. Math Biosci 180:141–160

Huang L, Wang J (2024) Global dynamics of piecewise smooth systems with switches depending on both discrete times and status. SIAM J Appl Dyn Syst 23:2533–2556

Kopfová J, Nábělková P, Rachinskii D, Rouf SC (2021) Dynamics of SIR model with vaccination and heterogeneous behavioral response of individuals modeled by the Preisach operator. J Math Biol 83:11
Krasnosel'skii MA, Pokrovskii AV (1989) Systems with Hysteresis. Springer-Verlag
Krejči P, O'Kane JP, Pokrovskii A, Rachinskii D (2012) Properties of solutions to a class of differential models incorporating Preisach hysteresis operator. Physica D 241:2010–2028
Leonov GA, Shumafov MM, Teshev VA, Aleksandrov K (2017) Differential equations with hysteresis operators: Existence of solutions, stability, and oscillations. Diff Equat 53:1764–1816
Liberzon D, Morse AS (1999) Basic problems in stability and design of switched systems. IEEE Control Syst Mag 19:59–70
Meza MEM, Bhaya A (2010) Control theory and the management of ecosystems: A threshold policy with hysteresis is robust. Appl Math Comput 216:3133–3145
Mondaini RP (2018) Trends in Biomathematics: Mathematical Modeling for Health, Harvesting, and Population Dynamics. Springer
Odagaki T (2020) Analysis of the outbreak of COVID-19 in Japan by SIQR model. Infect Dis Model 5:691–698
Pimenov A, Rachinskii D (2014) Homoclinic orbits in a two-patch predator-prey model with Preisach hysteresis operator. Math Bohem 139:285–298
Pimenov A, Kelly TC, Korobeinikov A, O'Callaghan MJA, Pokrovskii AV, Rachinskii D (2012) Memory effects in population dynamics: Spread of infectious disease as a case study. Math Model Nat Phenom 7:204–226
Pimenov A, Kelly TC, Korobeinikov A, O'Callaghan MJA, Rachinskii D (2015) Adaptive behaviour and multiple equilibrium states in a predator-prey model. Theor Popul Biol 101:24–30
Pimenov A, Kelly TC, Korobeinikov A, O'Callaghan MJA, Rachinskii D (2017) Memory and adaptive behavior in population dynamics: Anti-predator behavior as a case study. J Math Biol 74:1533–1559
Pinto CMA, Machado JAT, Burgos-Simón C (2024) Modified SIQR model for the COVID-19 outbreak in several countries. Math Methods Appl Sci 47:3273–3288
Rachinskii D, Rouf S (2022) Dynamics of SIR model with heterogeneous response to intervention policy. Theor Popul Biol 146:71–85
Schelling TC (1971) Dynamic models of segregation. J Math Sociol 1:143–186
Simpson D (2010) Bifurcations in Piecewise-Smooth Continuous Systems. World Scientific
Smith HL, Thieme HR (2011) Dynamical systems and population persistence. American Mathematical Soc
Visintin A (1994) Differential Models of Hysteresis. Springer
Wang H, Xiao Y (2025) A piecewise-smooth dynamic system with two thresholds and its application to epidemic control. Int J Bifurcat Chaos 35:2550122
Wang H, Xiao Y, Xiang C, Smith? SR, (2026) Classification of planar Filippov systems with a delayed threshold: Applications to infectious disease transmission dynamics. Nonlinear Anal Hybrid Syst 61:101711
Wang J, Zhang S, Wang L (2022) Global dynamics of a Filippov SIQR model with delayed relay control. SIAM J Appl Math 82:1879–1902
Wang K, Fan H, Zhu Y (2023) Dynamics and application of a generalized SIQR epidemic model with vaccination and treatment. Appl Math Modell 120:382–399
Wilder-Smith A, Chiew CJ, Lee VJ (2020) Can we contain the COVID-19 outbreak with the same measures as for SARS? Lancet Infect Dis 20:E102–E107
Wu L, Feng Z (2000) Homoclinic bifurcation in an SIQR model for childhood diseases. J Differential Equations 168:150–167

Publisher's Note Springer Nature remains neutral with regard to jurisdictional claims in published maps and institutional affiliations.

Springer Nature or its licensor (e.g. a society or other partner) holds exclusive rights to this article under a publishing agreement with the author(s) or other rightsholder(s); author self-archiving of the accepted manuscript version of this article is solely governed by the terms of such publishing agreement and applicable law.